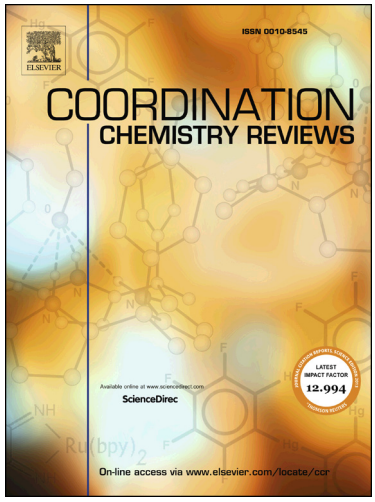

When defects turn into virtues: the curious case of zirconium-based metal-organic frameworks

Marco Taddei

PII: S0010-8545(17)30142-X
DOI: http://dx.doi.org/10.1016/j.ccr.2017.04.010
Reference: CCR 112445

To appear in: *Coordination Chemistry Reviews*

Received Date: 28 March 2017
Accepted Date: 27 April 2017

Please cite this article as: M. Taddei, When defects turn into virtues: the curious case of zirconium-based metal-organic frameworks, *Coordination Chemistry Reviews* (2017), doi: http://dx.doi.org/10.1016/j.ccr.2017.04.010

When defects turn into virtues: the curious case of zirconium-based metal-organic frameworks

Marco Taddei

Energy Safety Research Institute, College of Engineering, Swansea University, Fabian Way, Swansea, SA1 8EN, United Kingdom.

Email: marco.taddei@swansea.ac.uk

ABSTRACT

Zirconium-based metal-organic frameworks (Zr-MOFs) are one of the most attractive classes of MOF materials, due to their superior thermal, chemical and mechanical stability. Recently, Zr-MOFs have been shown to feature an unusually high concentration of defects without suffering from severe loss of stability. This feature makes Zr-MOFs unique among MOF materials and is generating additional interest around them. Defects have a significant impact on porosity, thermal properties, mechanical properties, Lewis and Brønsted acidity. Researchers have quickly recognized that defects can be engineered to tune the physical-chemical properties of Zr-MOFs, opening up new avenues for their practical application. The scope of the present review article is to provide a comprehensive account of the progress made in this field since the discovery of defects in Zr-MOFs in 2011 and to point out some relevant controversies and open issues of fundamental nature that need to be addressed to improve the understanding of the very nature of defects.

HIGHLIGHTS

- Zr-MOFs can contain many defects without suffering from loss of stability
- Defects significantly influence the physical-chemical properties of Zr-MOFs
- Gaps exist in the understanding of fundamental aspects of defects in Zr-MOFs
- Defects offer new opportunities for functionalization of Zr-MOFs

KEYWORDS

Metal-organic frameworks – Zirconium – Defects – Porous materials

Contents

LIST OF ABBREVIATIONS

MOF, metal-organic framework; Zr-MOF, zirconium-based metal-organic framework; H_2bdc, terephthalic acid; H_2bpdc, 4,4'-biphenyldicarboxylic acid; H_2tpdc, 4,4'-terphenyldicarboxylic acid; SBU, secondary building unit; H_3btc, 1,3,5-benzenetricarboxylic acid; H_4tbaPy, 1,3,6,8-tetrakis(p-benzoic acid)pyrene; H_2pzdc, 1*H*-pyrazole-3,5-dicarboxylate; DMF, *N,N*-dimethylformamide; PSM, Post-synthetic modification; TGA, thermogravimetric analysis; AA, acetic acid; SCXRD, single-crystal X-ray diffraction; BA, benzoic acid; PXRD, powder X-ray diffraction; FA, formic acid; PDF, pair distribution function; BET, Brunauer-Emmett-Teller; PA, propionic acid; *Q*st, isosteric heat of adsorption; DFT, density functional theory; DFA, difluoroacetic acid; TFA, trifluoroacetic acid; NMR, nuclear magnetic resonance; NTE, negative thermal expansion; CA, chloroacetic acid; CUS, coordinatively unsaturated site; SA, stearic acid; RH, relative humidity; AC, alternate current; Gly, glycine; *L*-Pro, *L*-proline; *L*-Phe, *L*-phenylalanine; DRIFTS, diffuse reflectance infrared Fourier transform spectroscopy; EDS, energy dispersive X-ray spectroscopy; PSE, post-synthetic exchange; H_4tcpp, tetrakis(4-carboxyphenyl)porphyrin; SALI, solvent assisted ligand incorporation; SLI, sequential linker installation; H_2Me_2-bpdc, 2,2'-dimethylbiphenyl-4,4'-dicarboxylic acid; H_2Me_2-tpdc, 2',5'-dimethylterphenyl-4,4''-dicarboxylic acid; PSDH, post-synthetic defect healing; PSDG, post-synthetic defect generation; PSDE, post-synthetic defect exchange; H_3sbdc, 2-sulfoterephthalic acid; SAXS, small angle X-ray scattering; WAXS, wide angle X-ray scattering; MOMO, metal-organic molecular orbital; *L*-Ser, *L*-serine.

1. Introduction

The discovery of zirconium-based metal-organic frameworks (Zr-MOFs) UiO-66, UiO-67 and UiO-68 in 2008 represented a milestone in MOF chemistry [1]. These MOFs have general formula $Zr_6O_4(OH)_4(L)_6$, where *L* can be either terephthalate (bdc^{2-}, UiO-66, Chart 1), 4,4'-biphenyldicarboxylate ($bpdc^{2-}$, UiO-67, Chart 1) or 4,4'-terphenyldicarboxylate ($tpdc^{2-}$, UiO-68, Chart 1), and their crystal structure is based on the connection of hexanuclear $[Zr_6O_4(OH)_4]^{12+}$ clusters *via* the bridging organic linkers, with each cluster connected to twelve other clusters (Figure 1). Since 2008, the same $[Zr_6O_4(OH)_4]^{12+}$ clusters have been combined with organic linkers having diverse geometrical and symmetrical features, giving rise to a large family of Zr-MOFs featuring a wide range of topologies (Figure 2) [2-7].

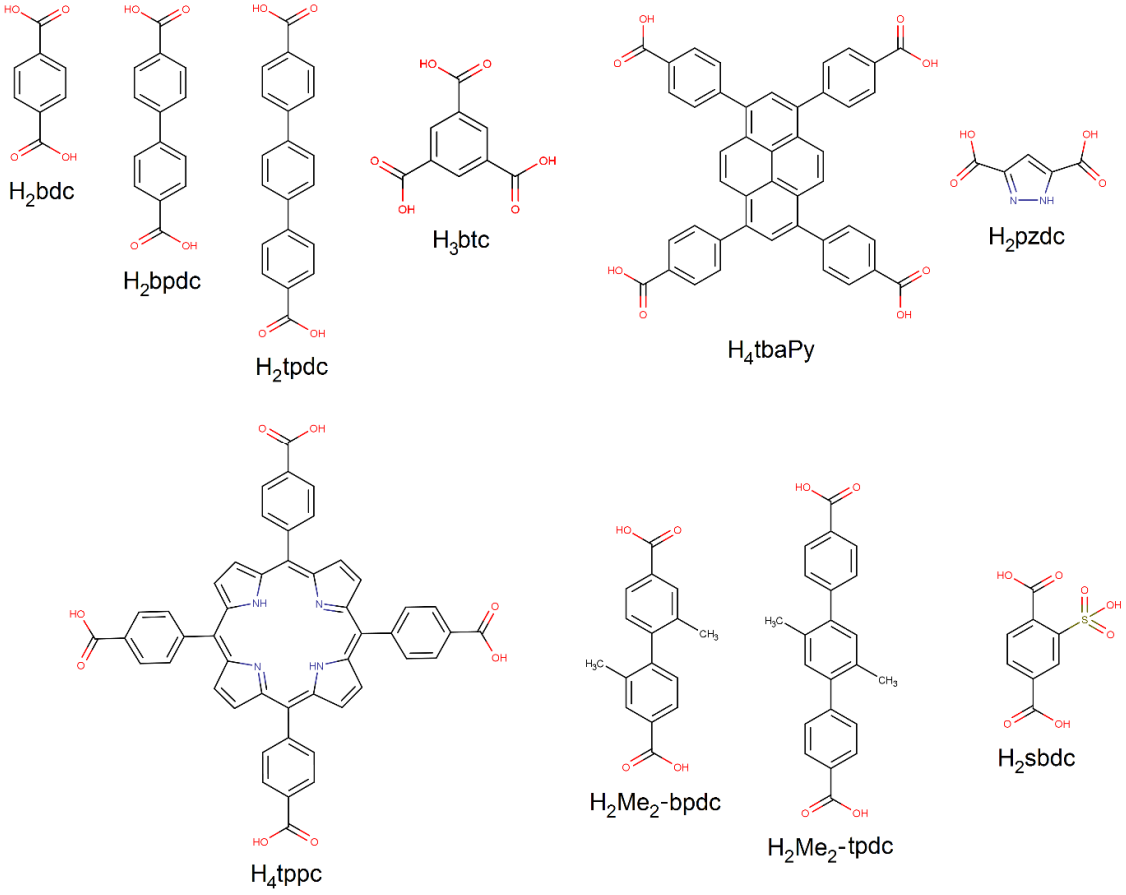

Chart 1. Molecular structure of the organic linkers cited in this review.

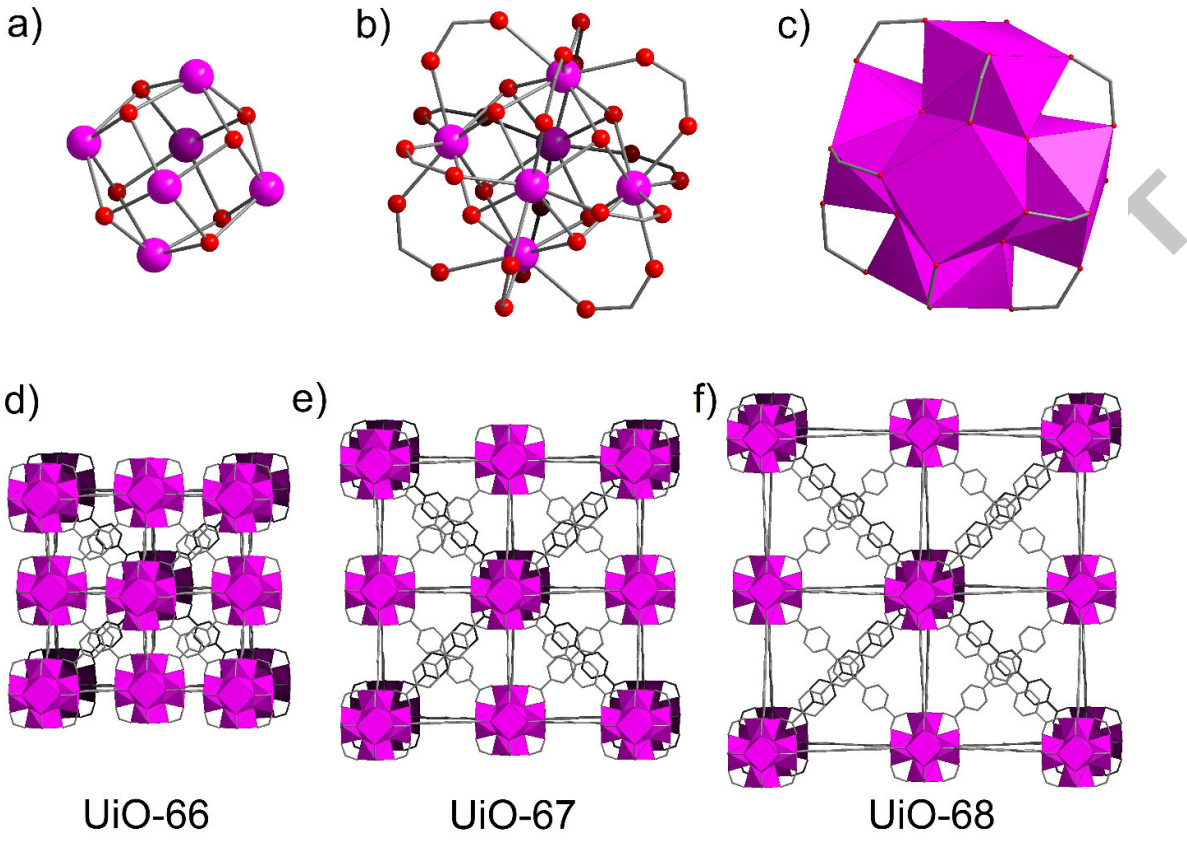

Figure 1. Representation of; the $[Zr_6O_4(OH)_4]^{12+}$ cluster (**a**), the $Zr_6O_4(OH)_4(COO)_{12}$ secondary building unit (SBU) (**b**) and a polyhedral representation of the SBU (**c**). Crystal structures of UiO-66 (**d**), UiO-67 (**e**) and UiO-68 (**f**) based on the connection of $[Zr_6O_4(OH)_4]^{12+}$ clusters *via* bdc^{2-}, $bpdc^{2-}$ and $tpdc^{2-}$, respectively. Colour code: ZrO_8 polyhedra, pink; O, red; C, grey. H atoms are omitted.

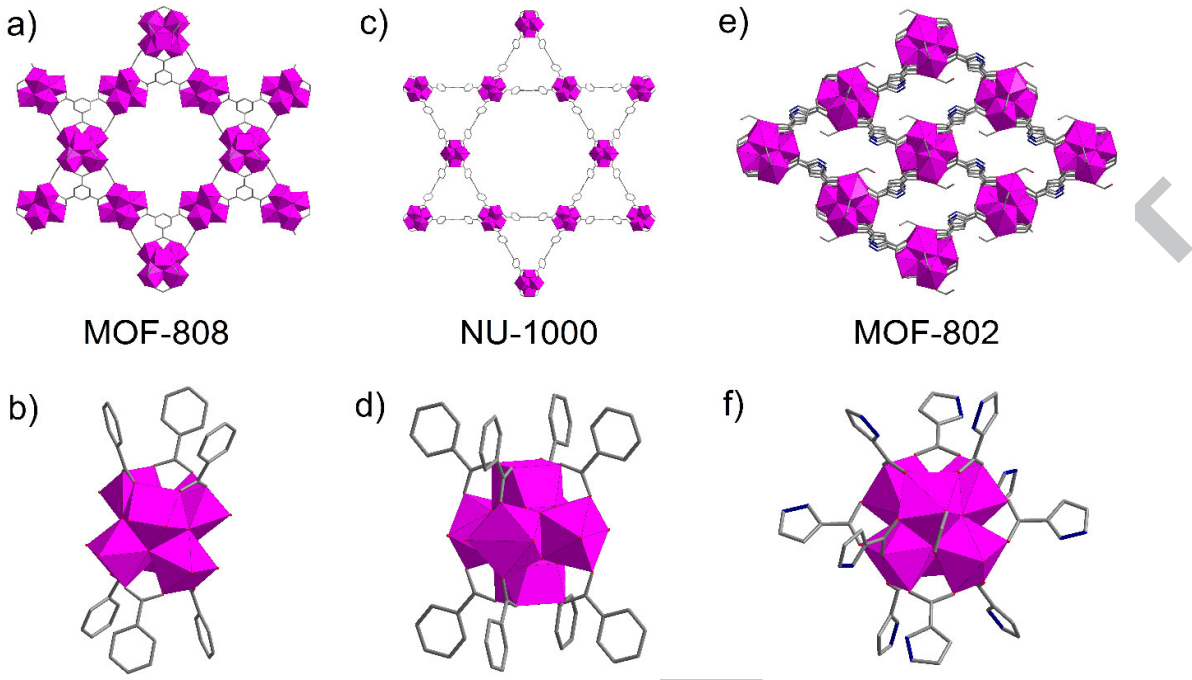

Figure 2. Crystal structures of representative Zr-MOFs based on clusters with degrees of connectivity lower than twelve: MOF-808 (**a**) is based on 1,3,5-benzenetricarboxylate (btc^{3-}) and six-connected clusters (**b**), giving rise to **spn** topology; NU-1000 (**c**) is based on 1,3,6,8-Tetrakis(*p*-benzoate)pyrene ($tbaPy^{4-}$) and eight-connected clusters (**d**), giving rise to **csq** topology; MOF-802 (**e**) is based on 1*H*-pyrazole-3,5-dicarboxylate ($pzdc^{2-}$) and ten-connected clusters (**f**), giving rise to **bct** topology. Colour code: ZrO_8 polyhedra, pink; O, red; C, grey; N, blue. H atoms are omitted.

Zr-MOFs display outstanding stability when compared to most of the known MOFs based on different metal ions or clusters: they are thermally stable up to 450 °C [1, 3, 5], can be soaked in many organic solvents and acidic aqueous solutions without suffering any significant damage [8, 9] and retain their crystal structure under high pressure [10, 11]. Such superior stability has been attributed to the strength of the carboxylate-Zr bond and to the high degree of connectivity of the metal clusters and is extremely attractive for practical applications. These applications include gas sorption/separation [12-16], heterogeneous catalysis [17-21], drug delivery [22-26], sensing [27-32] and electrochemistry [33-36].

The success of Zr-MOFs is also due to the ease and versatility of their synthesis [37]. This is demonstrated by the large number of new procedures that have been developed since the first solvothermal synthesis in *N,N*-dimethylformamide (DMF) [1]: water- [38-41], acetone- [42] and cyrene-based [43] synthesis, microwave-assisted synthesis [44-47], mechanochemical synthesis [48, 49], chemical vapor deposition [50], spray-drying [51], continuous flow synthesis [38, 52-56]. The use of monocarboxylic acids (Chart 2) or inorganic acids (HCl, HF) as modulators during synthesis is a

powerful tool that allows to obtain crystals with sizes ranging from the micrometer to the low nanometer range [57-63]. Compounds that cannot be prepared with the conventional synthetic approach are obtained *via* modulated synthesis [7, 64]. Isoreticular synthesis [18, 65-68] and mixed-linker synthesis [69-75] have been vastly explored with the aim of fine-tuning the physical-chemical features of Zr-MOFs, either by tailoring pore-size or by introducing multiple functional groups in the framework. Post-synthetic modification (PSM) [20, 76-85] also provides many opportunities to functionalize both the framework and the metal clusters. Thanks to these features, in less than ten years Zr-MOFs have become one of the most investigated subclasses of MOFs. The interested reader may refer to a recently published review by Zhou and co-workers for a comprehensive picture of the progress made in the field [2].

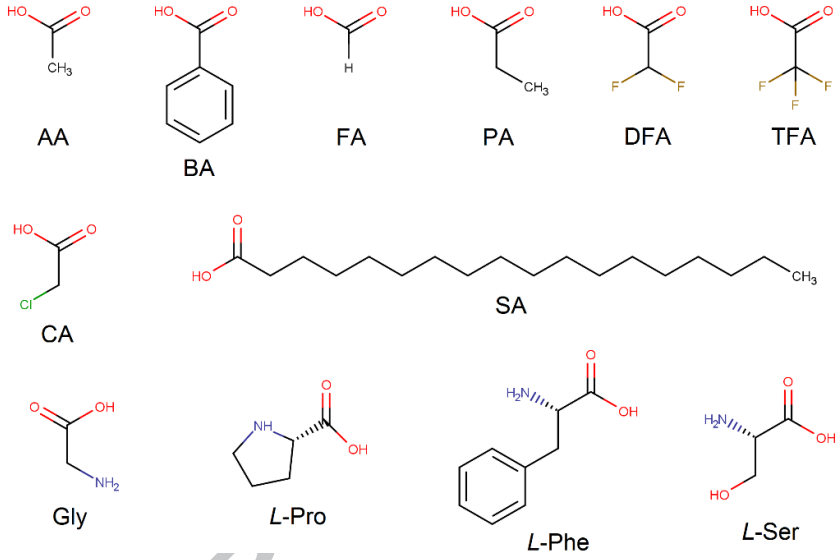

Chart 2. Molecular structure of the monocarboxylic modulators cited in this review.

Many MOFs, including Zr-MOFs, are known to contain defects and there is currently a great interest in understanding how these defects are formed and how they can be exploited for practical purposes [86-89]. Zr-MOFs are attracting particular attention thanks to the observation, first made in 2011 [90], that their crystal structure can contain unusually large amounts of defects without undergoing severe loss of stability. Two types of defects were discovered in Zr-MOFs: missing-linkers and missing-clusters (Figure 3).

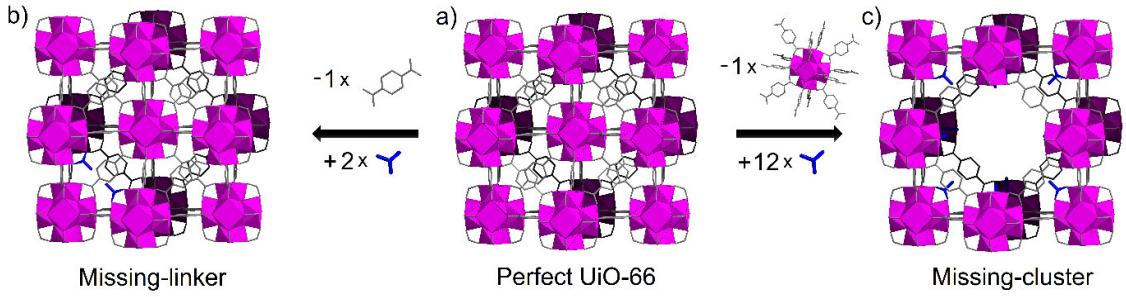

Figure 3. Idealized process of generation of defects in UiO-66 (**a**): replacement of one bdc^{2-} linker with two monocarboxylic groups (in blue), generating one missing-linker defect per unit cell (**b**) and replacement of one $Zr_6O_6(bdc)_{12}^{12-}$ unit with twelve monocarboxylic groups, generating one missing-cluster defect per unit cell (**c**). Colour code: ZrO_8 polyhedra, pink O, red; C, grey. H atoms are omitted.

Missing-linker defects are generated when an organic linker is removed from the structure, leaving coordination vacancies on two adjacent metal clusters [91] (Figure 3 **a** to **b**). Missing-cluster defects are the result of the removal of a $[Zr_6O_4(OH)_4]^{12+}$ cluster together with its entire set of twelve organic linkers, generating one coordination vacancy on the neighbouring clusters [92, 93] (Figure 3 **a** to **c**). The vacancies can be compensated by terminal ligands: either monocarboxylic ligands [91], which are often employed as modulators during the synthesis, or water [94], hydroxide [62], chloride [95] and fluoride [63]. From the solid state chemistry perspective, both types of defects in Zr-MOFs can be classified as vacancies, i.e. point defects, comparable to Schottky-type defects commonly found in ionic compounds [86, 87]. The high concentration of these defects is thought to be possible thanks to the high degree of connectivity of the metal clusters [90], which allows the removal of a large number of linkers or even clusters without causing collapse of the framework structure. The existence of "intrinsically defective" Zr-MOFs, containing clusters having lower degrees of connectivity than twelve, is a proof that structures based on the $[Zr_6O_4(OH)_4]^{12+}$ clusters can afford to be highly defective while preserving remarkable stability. Notable examples of such MOFs are shown in Figure 2: MOF-808, based on 1,3,5-benzenetricarboxylate (btc^{3-}, Chart 1) and featuring six-connected clusters [4], NU-1000, based on 1,3,6,8-Tetrakis(*p*-benzoate)pyrene ($tbaPy^{4-}$, Chart 1) and featuring eight-connected clusters [3], MOF-802, based on 1*H*-pyrazole-3,5-dicarboxylate ($pzdc^{2-}$, Chart 1) and featuring ten-connected clusters [4]. From a crystallographic point of view, these Zr-MOFs would not be considered as defective solids, due to the ordered nature of their framework that makes every single unit cell in their crystal structure identical to the bulk. However, for the sake of this review they are included in the class of defective Zr-MOFs, based on the fact that the

physical-chemical features (and the resulting behaviour) of the metal clusters found in their structure are indistinguishable from those of clusters found in "properly defective" Zr-MOFs.

After 2011, researchers have engaged in intense activity devoted to unravel fundamental aspects of defective Zr-MOFs, driven by an interest in gaining the ability to harness the defects to tune the physical-chemical properties of Zr-MOFs, ultimately targeting practical applications. The present account is intended to provide a critical review of the most important advancements made to date, to point out some controversies and open issues that need to be addressed by the community and to delineate some of the most promising new directions for the future.

2. A brief history of the discovery of defects in Zr-MOFs

The first indication of the presence of defects in Zr-MOFs came from thermogravimetric analysis (TGA) of UiO-66 [90]. The TG curve of UiO-66 displays three main steps: i. removal of solvent molecules from the porous framework (desolvation) is usually complete at T < 150 °C; ii. removal of two water molecules per $[Zr_6O_4(OH)_4]^{12+}$ cluster leading to $[Zr_6O_6]^{12+}$ clusters occurs at T < 300 °C (dehydroxylation); iii. decomposition of the organic part of the desolvated and dehydroxylated MOF to yield ZrO_2 takes place at T > 450 °C. It was observed that the TG curves of different batches of UiO-66 displayed significant differences in the extent of the weight loss occurring at T > 450 °C (Figure 4). More specifically, most of the samples experienced a smaller weight loss than expected from the ideal chemical formula $Zr_6O_6(bdc)_6$ of a desolvated and dehydroxylated UiO-66 sample. The authors attributed this discrepancy to the existence of missing-linker defects in the framework, speculating that either hydroxide anions or DMF molecules could fill the vacancies left on the clusters.

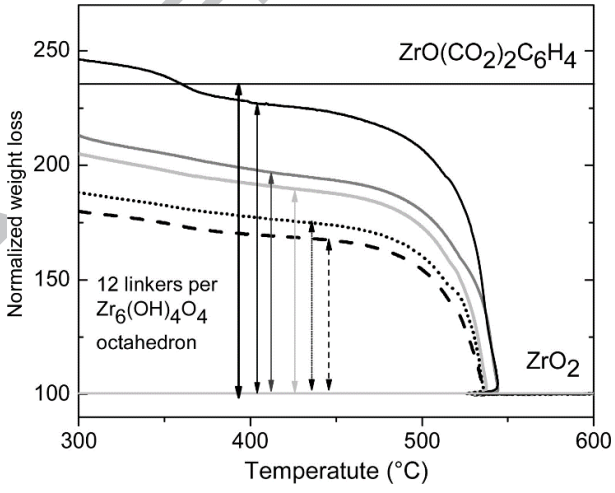

Figure 4. TG curves of five independently prepared UiO-66 batches (solid black line, solid dark grey line, solid light grey line, dotted black line, dashed black line; experimental conditions not specified in the original publication) showing different weight losses upon decomposition of the organic part of the framework. The ordinate axis is normalized to 100 for the ZrO_2 residual at high temperature. The horizontal black line marks the ideal weight loss for a non-defective sample. [Reprinted with permission from ref. [90]. Copyright 2011, American Chemical Society.]

Two years later, direct structural evidence of the presence of missing-linker defects in UiO-66 was provided by performing high-resolution neutron diffraction study on a sample containing deuterated bdc^{2-} linkers [91]. The authors assumed that defects were randomly distributed throughout the crystal structure, a situation that can be crystallographically described by employing the structural model of the ideal defect-free UiO-66 (cubic, space group *Fm*-3*m*) and refining the occupancy of the linkers' atoms. The best fit to the experimental data was obtained when the occupancy of the linkers was 91.7%, corresponding to about one missing linker per cluster. In the same article, the authors reported that the number of missing-linker defects could be tuned by employing different amounts of acetic acid (AA, Chart 2) as a modulator during the synthesis. Evidence for this came from the increased pore volume of samples prepared in the presence of larger amounts of AA, suggesting the presence of more missing linkers. The authors speculated that AA could promote the formation of defects by substituting bdc^{2-} linkers on the clusters and provided evidence based on inelastic neutron scattering measurements.

Further insight on missing-linker defects came from single-crystal X-ray diffraction (SCXRD). A study on single crystals of UiO-66 and UiO-67 prepared in analogous conditions using benzoic acid (BA, Chart 2) as a modulator showed a remarkable difference between the two compounds [61]: while UiO-66 featured as much as 27% of missing linkers, UiO-67 was practically defect-free. The irregular electron densities around defective clusters in UiO-66 suggested that local disorder existed due to missing linkers, but this did not apparently translate into a relevant loss of long-range order and the structure preserved its face-centered cubic symmetry. The presence of benzoate as a vacancy-filling species in UiO-66 was excluded based on the refined structure, assuming that a mixture of water, hydroxide anions and DMF could act as compensating groups (Figure 5).

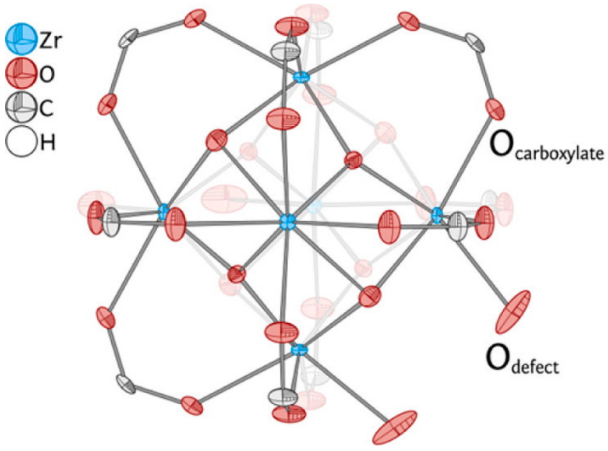

Figure 5. Ellipsoid model of a defective cluster in UiO-66, as obtained from SCXRD data. Large irregularities in the electron density map around the carboxylate oxygen of the linker ($O_{carboxylate}$) were described by adding another oxygen atom corresponding to either –OH or H_2O compensating species (O_{defect}). $O_{carboxylate}$ and O_{defect} sit on nearby positions and have inverse occupancies, adding up to a total of 100%. [Reprinted with permission from ref. [61]. Copyright 2014, American Chemical Society.]

While it was initially assumed that defects existed in the form of randomly distributed missing linkers, a paper published in 2014 opened up a new scenario. In this work, the presence of weak and broad superlattice reflections in the powder X-ray diffraction (PXRD) pattern of hafnium-based UiO-66 [UiO-66(Hf)] was unambiguously attributed to the existence of a secondary crystalline phase having practically the same unit cell size but lower symmetry (cubic, space group *Pm*-3*m*, *a* = 20.712 Å) than the main UiO-66 phase (cubic, space group *Fm*-3*m*, *a* = 20.7339 Å) (Figure 6).

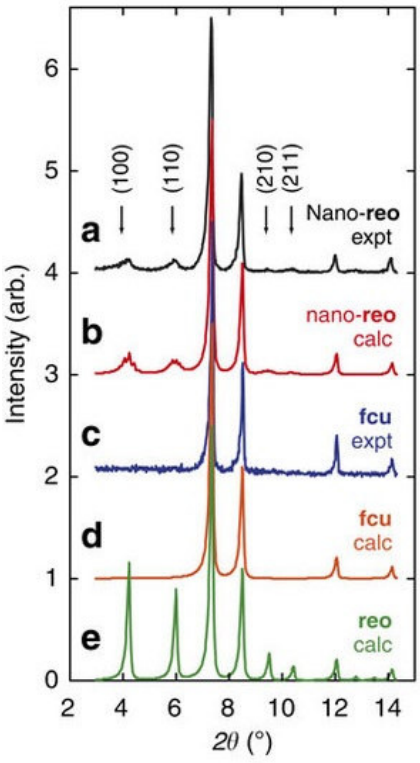

Figure 6. The experimental PXRD pattern of a UiO-66(Hf) sample containing correlated missing-cluster defects shows a sharp Bragg component corresponding to the reflections of a face-centred cubic cell (**fcu** topology) and a secondary broad component associated with superlattice reflections (**reo** topology, Miller indices are displayed) indicative of a primitive symmetry (**a**, black). Simulated PXRD pattern on the basis of a model featuring an **fcu** matrix containing nanodomains having **reo** topology (**b**, red). Experimental (**c**, blue) and calculated (**d**, orange) PXRD patterns of a defect-free sample having pure **fcu** character and no diffuse scattering features. Calculated PXRD pattern for a long-range ordered **reo** phase (**e**, green). [Reprinted with permission from ref. [92]. Copyright 2014, Nature Publishing Group.]

The intensity of the superlattice reflections was dependent on the amount of formic acid (FA, Chart 2) used as a modulator during the synthesis and TGA suggested that more defects were generated when larger amounts of FA were employed. A combination of pair distribution function (PDF) analysis, anomalous X-ray scattering at the Hf K-edge and electron diffraction suggested that the symmetry lowering results from the removal of one cluster and all the twelve linkers connected to it from the unit cell of UiO-66. This gives rise to a framework having **reo** topology, where each cluster is eight-connected and formate ligands fill the defective sites, according to the formula $Hf_6O_4(OH)_4(bdc)_4(HCOO)_4$ (Figure 7).

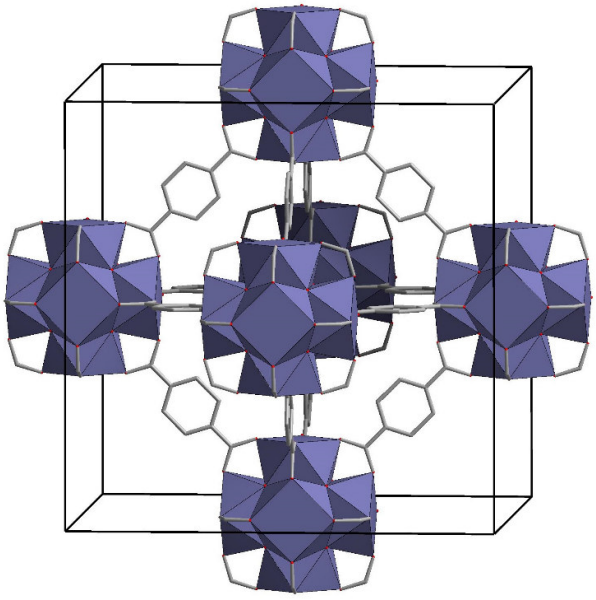

Figure 7. Polyhedral representation of the unit cell of a UiO-66(Hf)-type **reo** defect structure having $Hf_6O_4(OH)_4(bdc)_4(HCOO)_4$ formula. This structure is generated upon removal of the clusters sitting on the corners of the **fcu** unit cell along with their linkers (see figure 1d for comparison). Colour code: HfO_8 polyhedra, blue-grey; O, red; C, grey. H atoms are omitted.

As a result, octahedral cages having diameter of about 18 Å are generated in the framework in addition to the usual tetrahedral (d = 7 Å) and octahedral (d = 9 Å) ones found in UiO-66. This missing-cluster defective phase exists in the form of nanodomains, consisting of a few unit cells, embedded in a defect-free matrix having the usual **fcu** topology of UiO-66 (Figure 8), as revealed by the corresponding broad reflections in the PXRD pattern. An important aspect emerging from this work is that missing-cluster defects in UiO-66(Hf) were formed in a correlated fashion, i.e. the presence of a defective site increased the probability of formation of another defect at neighbouring sites, potentially generating local defect fields that could have significant influence on the material's properties.

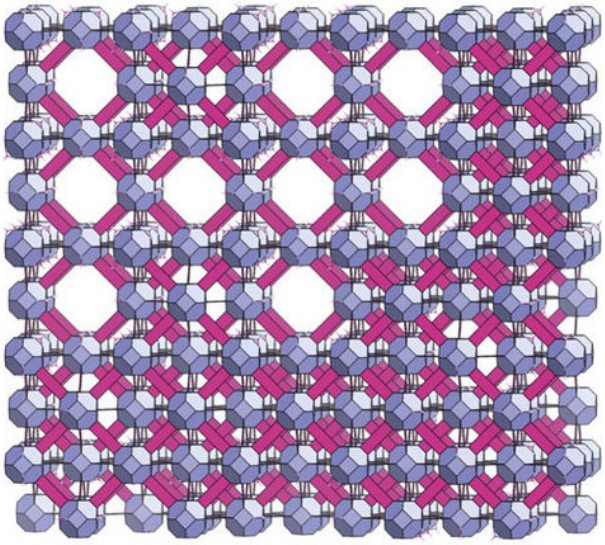

Figure 8. Simulated model of a defective UiO-66(Hf) framework highlighting the correlated nature of the **reo**-type missing-cluster defective nanodomains. $[Hf_6O_4(OH)_4]^{12+}$ clusters are represented as blue-grey truncated octahedra, bdc^{2-} linkers are represented as magenta bricks. [Reprinted with permission from ref. [92]. Copyright 2014, Nature Publishing Group.]

3. Impact of defects on the physical-chemical properties of Zr-MOFs

3.1 Gas sorption properties

The most obvious consequence of the presence of defects in Zr-MOFs is the increase of their pore volume and surface area: removing either linkers or clusters results in generating larger cavities in the crystal structure and in decreasing the density of the material. This allows the introduction of larger amounts of guest gaseous species per unit of mass as more defects are generated in the framework.

It was quickly shown that the micropore volume and Brunauer-Emmett-Teller (BET) surface area of UiO-66 could be tuned upon addition of different amounts of AA as a modulator in the synthesis, ranging between 0.42 $cm^3\ g^{-1}$ and 1090 $m^2\ g^{-1}$, respectively, when no AA was used, up to 0.59 $cm^3\ g^{-1}$ and 1558 $m^2\ g^{-1}$, respectively, when 70 equivalents of AA were present in the reaction mixture (Figure 9) [91].

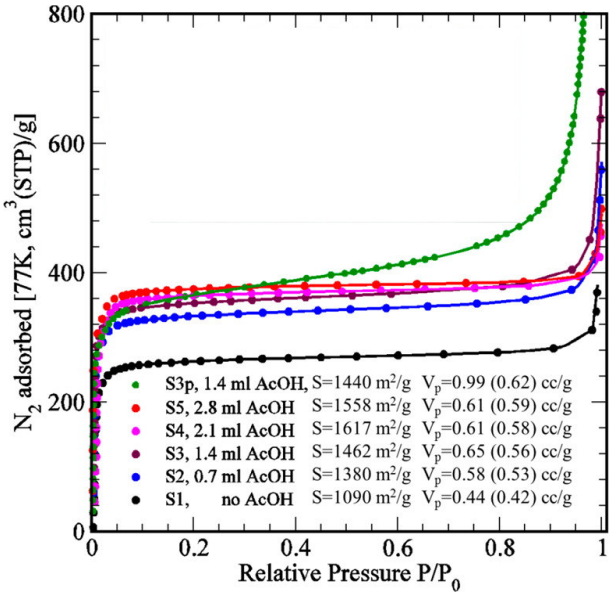

Figure 9. Nitrogen sorption isotherms and corresponding BET surface area and pore volume of UiO-66 samples prepared in the presence of different amounts of AA as a modulator. [Reprinted with permission from ref. [91]. Copyright 2013, American Chemical Society.]

The effect of different monocarboxylic compensating groups on the porosity of MOF-808 was investigated [96]. The MOF was synthesized employing FA, AA and propionic acid (PA, Chart 2), observing that the nature of the vacancy-filling monocarboxylates did not affect thermal and chemical stability, but had a significant influence on porosity. The BET surface area decreases from 2330 $m^2 g^{-1}$ when FA is incorporated, to 1606 $m^2 g^{-1}$ when AA is incorporated, down to 1408 $m^2 g^{-1}$ when PA is incorporated. Pore size distribution analysis clearly displays that pore diameter decreases from 15.2 Å to 14.2 Å as the length of the side chain increases.

However, defects can influence the gas sorption properties of Zr-MOFs also by affecting the chemical environment inside the porous structure, especially when more interactive species than nitrogen are concerned. It was demonstrated that the uptake of CO_2 and H_2O in UiO-66 can be tuned by engineering the defects [46]. Samples of defective UiO-66 by using either HCl or FA as modulators were prepared. Nitrogen sorption analysis reveals that samples obtained with increasing amounts of modulators have increasing BET surface area and pore volume, exceeding those observed for a sample prepared without modulator and suggesting the presence of defects when modulators are employed. However, the CO_2 uptake at 1 bar and 298 K is lower for defective UiO-66 than for the defect-free material and it decreases as the number of defects increases, suggesting that enlarged cavity size is detrimental for CO_2 adsorption (Figure 10a). A different trend is observed for the CO_2 isosteric heats of adsorption (*Q*st) (Figure 10b): the *Q*st of the HCl-modulated samples is higher than that of defect-free UiO-66, which is in turn higher than those for the FA-modulated samples. Such a

trend was interpreted as an evidence of more favourable interaction of CO_2 molecules with –OH and –Cl groups than with –OOCH groups at defective sites. Density functional theory (DFT) calculations support this interpretation, showing that the binding energy for CO_2 to the Zr clusters decreases in the order -OH > -Cl > perfect > -OOCH. The presence of defects was also found to increase the hydrophilicity of UiO-66, as already predicted based on calculations [97]. The removal of hydrophobic bdc^{2-} linkers most likely plays the main role in increasing the affinity for water: as a matter of fact, in this case the water uptake is a direct function of the number of defects and no influence of the compensating groups is observed (Figure 10d).

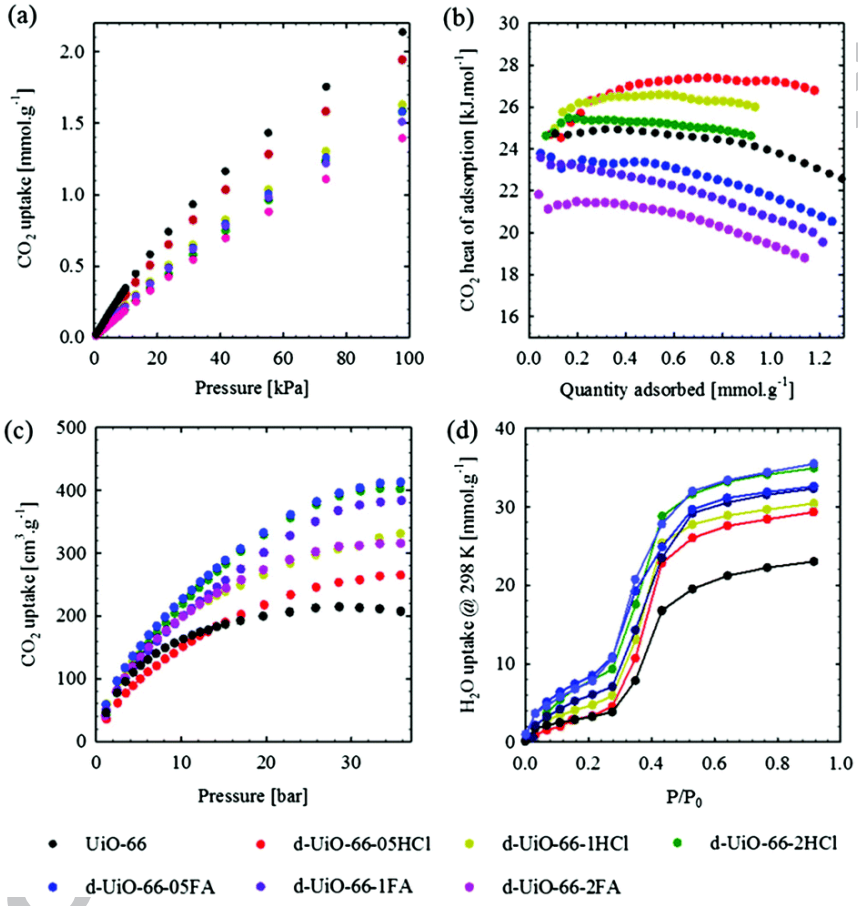

Figure 10. CO_2 adsorption isotherms measured at 298 K up to 1 bar (**a**), isosteric heat of CO_2 adsorption (**b**), CO_2 adsorption isotherms measured at 298 K up to 35 bar (**c**) and water adsorption isotherms measured at 298 K (**d**) for defect-free UiO-66 (black), UiO-66 synthesized with addition of 0.5 mL (red), 1 mL (yellow) and 2 mL of HCl (green), UiO-66 synthesized with addition of 0.5 mL (blues), 1 mL (violet) and 2 mL of FA (purple). [Reprinted with permission from ref. [46]. Copyright 2016, Royal Society of Chemistry.]

3.2 Thermal properties

MOFs undergo irreversible thermal degradation when the metal–linker bonds break, accompanied or followed by linker combustion [98]. Thermal stability is therefore a consequence of the metal–linker bond strength and of the number of linkers connecting metal ions or clusters. Zr-MOFs feature both strong Zr-carboxylate bonds and a high degree of connectivity of the framework, which confer a remarkable resistance to thermal degradation. This suggests that loss of connections between $[Zr_6O_4(OH)_4]^{12+}$ clusters can negatively impact on the thermal stability.

The effect of defects on the thermal properties of UiO-66 was thoroughly investigated in 2014 [95]. Three series of samples were prepared using a fixed amount of HCl as a modulator and varying temperature (100, 160 and 220 °C), linker to metal ratio (1:1, 5:4, 3:2, 7:4, 2:1) and workup procedures (one or two washing cycles with either DMF or methanol), finding that the amount of defects is a function of each of the above parameters. More specifically, syntheses performed at lower temperature and linker to metal ratio yield more defective materials, as displayed by: 1. the increased intensity of the superlattice reflections associated with the **reo**-type missing-cluster phase in the PXRD pattern; 2. the lower weight loss upon decomposition of the organic part of the framework in the TGA curve. Despite all the samples undergo thermal decomposition of the organic part of the framework at about 450 °C, significant differences can be observed in the PXRD patterns collected after thermal treatment at different temperatures (Figure 11). In fact, more defective UiO-66 suffers significant loss of long-range order at 250 °C, whereas the defect-free sample fully retains its crystallinity up to 450 °C. In addition, the stability of defective UiO-66 is significantly affected by repeated washing with solvents.

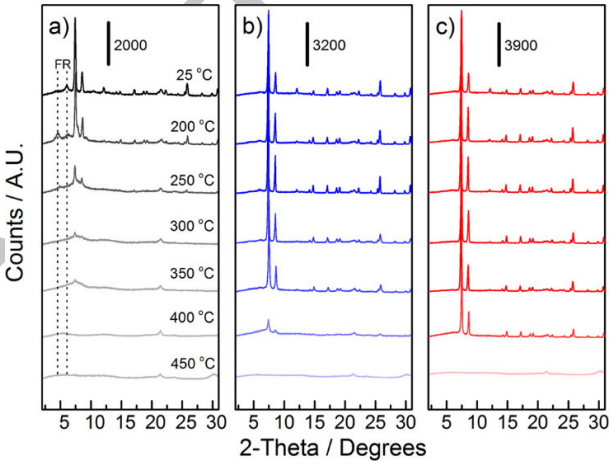

Figure 11. PXRD patterns of UiO-66 samples prepared at 100 °C (black), 160 °C (blue) and 220 °C (red), recorded after heating at different temperatures for 12 h. The reflections labelled “FR” and

traced by dotted lines in the leftmost plot are related to the **reo** defective phase. [Reproduced with permission from ref. [95]. Copyright 2014, American Chemical Society.]

Two years later, the same authors published another study where the effect of different monocarboxylic acid modulators [FA, AA, difluoroacetic acid (DFA, Chart 2) and trifluoroacetic acid (TFA, Chart 2)] on the defectivity was investigated [93]. It turns out that the most acidic modulators DFA and TFA induce the formation of a much larger number of defects. This is probably due to the presence of large amounts of deprotonated modulator molecules in the reaction mixture, which can compete more effectively with the linker. However, the thermal stability of the defective MOFs is not as heavily affected as when HCl is employed in the synthesis and no significant loss of crystallinity occurs below 350 °C. Nuclear magnetic resonance (NMR) analysis of the samples dissolved in 0.1 M NaOH in D_2O displays the signals of modulator species, suggesting that they are in fact present in the framework as defect-compensating groups, probably contributing to preserve it from collapse at high temperature.

Following the report on the existence of correlated defective nanoregions with **reo** topology in UiO-66(Hf) [92], the same authors demonstrated that defects have an influence on thermal densification and negative thermal expansion (NTE) of the framework and that the magnitude of these phenomena is a function of defect concentration [99]. Thermal densification, i.e. decrease of cell volume upon heating, is a result of removal of formate compensating groups between 250 and 350 °C, with the most defective sample exhibiting an effect larger by 1% than that observed for the least defective one. All samples undergo NTE when cooled from 340 to 100 °C, although this phenomenon shows inverse relationship to defect concentration. In particular, the least defective sample displays "colossal" NTE in the temperature range investigated, as indicated by the value of its lattice expansivity of -97 MK^{-1} (Figure 12).

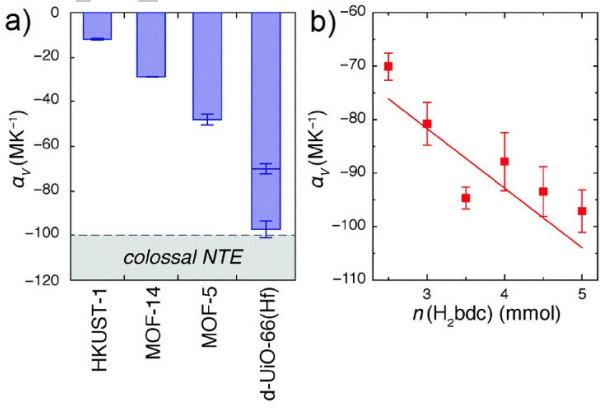

Figure 12. Coefficients of thermal expansion (a_V) for isotropic NTE MOFs (**a**) and variation of the same coefficient as a function of the amount of H_2bdc in the reaction mixture (the larger the amount of H_2bdc, the lower the defectivity of the product) (**b**). [Reprinted from Ref. [99] with permission from the PCCP Owner Societies. Copyright 2016, Royal Society of Chemistry.]

3.3 Mechanical properties

The ability to withstand high pressures without undergoing significant structural change and/or collapse is a key feature to enable processing of MOF powders into industrially viable forms, such as pellets and extrudates [100-102]. If compared with most other MOF materials, Zr-MOFs display an outstanding structural stability when exposed to high pressure [10, 11]. However, similar to thermal stability, the removal of connections between clusters can significantly impact on the mechanical properties of the framework.

The effect of defects on the high-pressure behaviour of UiO-66 was recently evaluated with the aid of DFT-based simulations [103]. Models featuring an average number of missing-linker defects from zero to four were investigated, finding that anisotropy increases with the number of defects, causing loss of stability (Figure 13). The **reo**-type structure, where ordered missing-cluster defects exist, represents a notable exception, being much more stable than the corresponding structure where four linkers per cluster are randomly removed. In addition, various compensating groups were considered, observing that the incorporation of acetate and trifluoroacetate contributes to strengthening the MOF if compared with scenarios where formate, hydroxyl or chloride are coordinated at defective sites. Shortly thereafter, it was demonstrated that the presence of TFA as compensating group in fact greatly enhances the resistance of defective UiO-66 to prolonged ball milling [104]. The collapse time, i.e. the time at which complete amorphization occurs, increases from 5-10 minutes for a UiO-66 sample prepared without modulator to 180 min for the MOF containing TFA (Table 1). AA and chloroacetic acid (CA, Chart 2) were also tested as modulators, finding that the collapse times are inversely related to the pK_a of the modulator. Stabilization was ascribed to a local electron-withdrawing effect exerted by the coordinated modulator that increases the partial positive charge on the metal atom, thus strengthening the Zr-linker bonds.

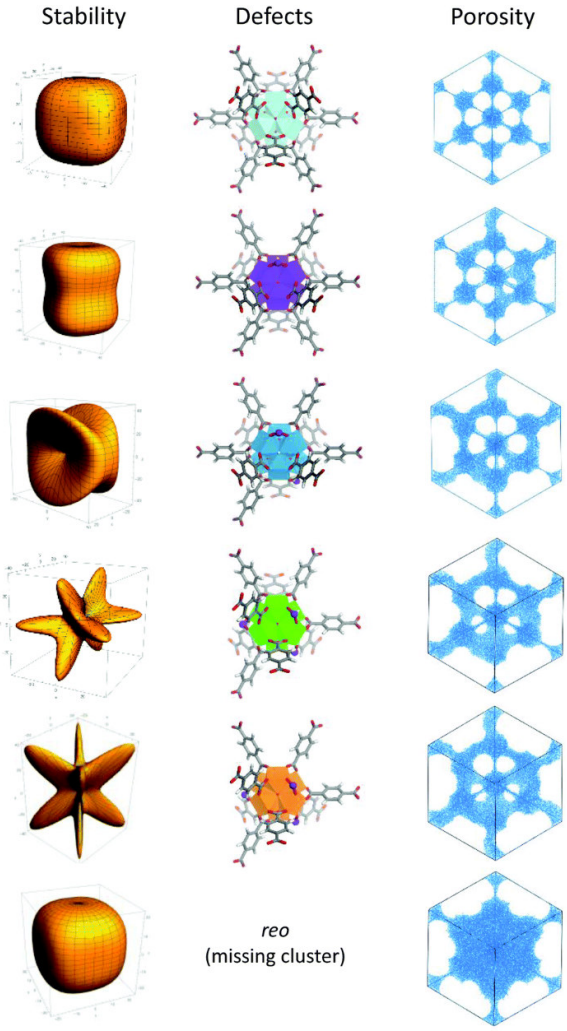

Figure 13. Calculated spatially-dependent Young's modulus (left) and accessible porosity to a probe having 3 Å diameter (right) for different defective UiO-66 models where each cluster has coordination number 12 (light blue), 11 (purple), 10 (dark blue), 9 (green) and 8 (orange) (center). O atoms are represented in red, C atoms in grey. H atoms are omitted. [Reprinted with permission from ref. [103]. Copyright 2016, Royal Society of Chemistry.]

Table 1. Comparison of the collapse time of different modulated and non-modulated UiO-66, showing its dependence on the pK_a of the modulator. [Adapted from ref. [104]. Copyright 2015, Royal Society of Chemistry.]

	UiO-66(TFA)	UiO-66(CA)	UiO-66(TFA)-HT[a]	UiO-66	UiO-66(AA)
pK_a of the modulator	≈ 0	2.86	-	-	4.76
Collapse time (min)	> 180	10	5-10	5-10	< 5

[a] TFA-modulated UiO-66 treated at 350 °C to remove TFA from the clusters.

Another computational approach aimed at disclosing correlations between defects and mechanical properties was reported [105], in which pressure-versus-volume curves derived from a force-field-based procedure were constructed. The authors simulated unit cells of UiO-66 without defects and with one and two missing linkers, respectively. In the latter case, seven possible scenarios were considered, featuring different distance between defects, relative orientation and coordination number of the inorganic clusters. Calculations predict that both the bulk modulus and the loss-of-crystallinity pressure decrease from 22.2 GPa and 1.83 GPa, respectively, for defect-free UiO-66, to 19.9 GPa and 1.55 GPa when one linker is missing, to 15.5-18.9 GPa and 1.17-1.38 GPa when two linkers are removed (Figure 14). The large range of values found for the most defective case suggests that not only the number of linker vacancies, but also their relative orientation plays a role in determining the mechanical behaviour of the MOF.

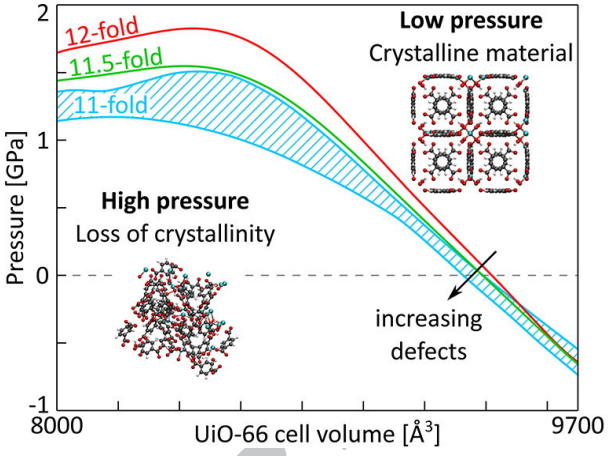

Figure 14. Internal pressure as a function of the constrained unit-cell volume at 300 K for UiO-66 models containing clusters with average coordination number 12 (defect-free; red), 11.5 (green) and 11 (seven unique models covering a range of values; light blue). Loss-of-crystallinity pressures for each model correspond to the maximum of the relative curve. [Reprinted from ref. [105]. Copyright 2016, American Chemical Society.]

3.4 Lewis acidity

The presence of Lewis acid sites in MOFs has been demonstrated to be very important for both gas sorption [106, 107] and catalytic purposes [17, 108, 109]. $[Zr_6O_4(OH)_4]^{12+}$ clusters are prone to undergo dehydroxylation upon treatment of at 300 °C under vacuum, leading to the formation of $[Zr_6O_6]^{12+}$ clusters, where each Zr atom is seven-fold coordinated and has Lewis-acid character (Figure 15) [90, 110]. These sites were found to be active as catalysts for the cross-aldol

condensation reaction [21]. Different functional groups attached to the linker had an influence on acid strength and catalytic activity [111]. The introduction of defects is a strategy to increase the number of Lewis acid sites and has primarily been exploited for catalytic applications.

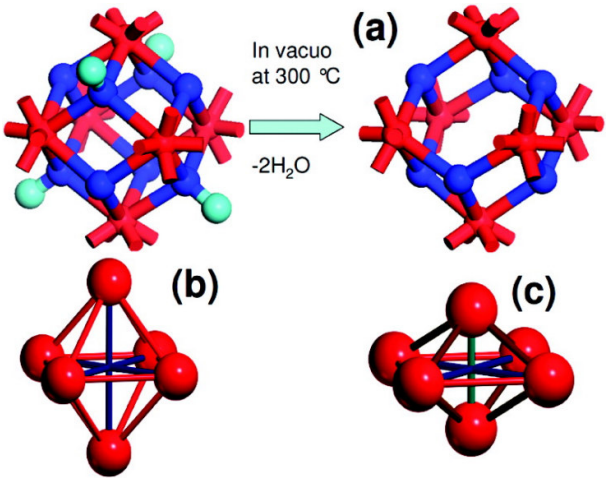

Figure 15. Simulated loss of two water molecules at 300 °C under vacuum from a $[Zr_6O_4(OH)_4]^{12+}$ cluster to yield a dehydroxylated $[Zr_6O_6]^{12+}$ cluster (**a**). Dehydroxylation induces a decrease of symmetry of the Zr_6 octahedron from a perfect (**b**) to a "squeezed" shape (**c**). Colour code: Zr, red; O, blue; H, light blue. [Reproduced with permission from ref. [90]. Copyright 2011, American Chemical Society.]

An approach based on the use of TFA as a modulator was reported, which yields a defective framework incorporating trifluoroacetate groups as vacancy fillers at defective sites (Figure 16) [112]. Removal of TFA upon treatment at 320 °C under vacuum generates coordinatively unsaturated sites (CUS) on the clusters which are active as Lewis acids for the catalytic conversion of citronellal. The catalytic activity is further increased by combined use of TFA and HCl during the synthesis, which favours incorporation of more TFA and therefore generation of more CUS upon thermal activation. The authors also demonstrated that the enlargement of pore size upon defect creation is crucial to catalyse the Meerwein-Ponndorf–Verley reaction of 4-tert-butylcyclohexanone and isopropanol, where both reagents need to be simultaneously activated to allow the reaction to happen.

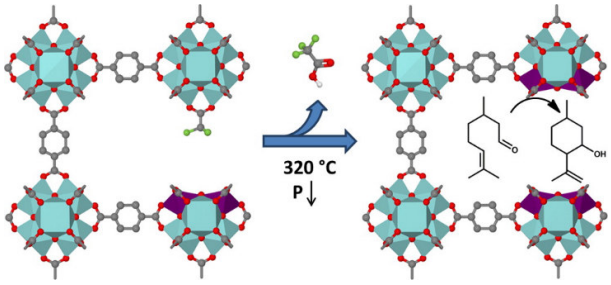

Figure 16. Pictorial representation of the removal of TFA grafted at defective sites in UiO-66 upon heating at 320 °C and under vacuum, leading to formation of catalytically active Lewis-acidic CUS for the cyclization of citronellal. Colour code: ZrO_8 polyhedra, light blue; ZrO_7 polyhedra, violet; O, red; C, grey; F, green. H atoms are omitted. [Reprinted with permission from ref. [112]. Copyright 2013, American Chemical Society.]

A theoretical study aimed at gaining further insight into the thermodynamic aspects of defects formation and their catalytic implications followed shortly thereafter [113]. In this work, the authors demonstrated that the structure incorporating two trifluoroacetate groups in place of one linker is energetically reachable, although less stable than the defect-free structure by 85.9 kJ mol^{-1}. Other structures where either –Cl or –OH groups acted as compensating groups are considerably less accessible, supporting the experimental evidence that TFA is preferably incorporated as a defect-filling species. Removal of TFA upon treatment at 320 °C and 10^{-3} bar was also simulated, confirming that in these conditions the process is thermodynamically favourable, leaving CUS on the clusters.

The effectiveness of Zr-MOFs for the catalytic decomposition of phosphate-based chemical warfare agents was demonstrated and Lewis acid sites in the clusters were identified as the active sites [114]. In the case of NU-1000, based on eight-connected clusters where one water molecule and one hydroxide group fill each remaining defective site, a significant increase of the catalytic activity results from formation of Lewis acid sites upon dehydration of the clusters. The authors exploited a similar approach on UiO-66 and UiO-67, synthesizing defective samples containing water and hydroxide as compensating groups, finding that also in this case dehydration leads to enhanced catalytic activity towards the hydrolysis of methylparaoxon [115]. The dependence of the catalytic activity on pH was investigated, finding that it decreases at pH > 8.8. This is in apparent contrast with the fact that hydrolysis occurs upon attack of a hydroxide anion on the substrate. To explain this evidence, the authors proposed a mechanism (Figure 17) where the nerve agent coordinates to the Zr atom *via* its P=O group and substitutes a water molecule. This weakens P-O bonds, making them more prone to hydrolysis. At pH > 8.8, deprotonation of the neutral water molecules coordinated to

the clusters leads to formation of anionic -OH species, which are more strongly bound and harder to replace with the nerve agent.

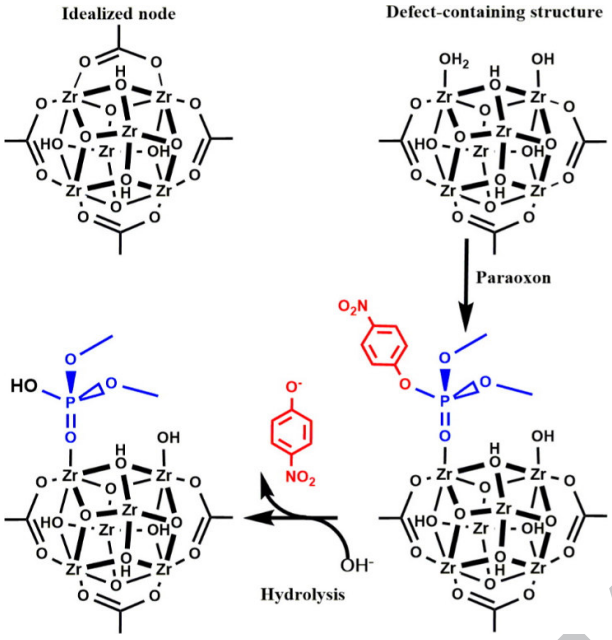

Figure 17. Proposed mechanism for methylparaoxon degradation in a defective Zr-MOF with OH^- /H_2O as compensating species. First step is substitution of water coordinated to the clusters with methylparaoxon, followed by hydrolysis of the P-O bond by OH^- and release of *p*-nitrophenolate. [Reprinted with permission from ref. [115]. Copyright 2015, American Chemical Society.]

3.5 Brønsted acidity

Brønsted acid sites can be exploited for applications such as catalysis [116], selective sorption of hazardous species, e.g. ammonia [117], and proton-conductive materials [118]. However, Brønsted acid chemistry has not been largely explored in MOFs, due to the limited chemical stability of most of them [119]. In virtue of their superior robustness, Zr-MOFs are ideal MOF platforms for introduction of Brønsted acidic sites. Defect-free Zr-MOFs have a weak Brønsted acid character due to the presence of μ_3-OH groups in the clusters, but additional sites can be introduced by creation of defects.

Acid-base titration experiments were carried out on perfect samples of UiO-67, observing a single equivalent point at pH = 7.1 and calculating a pK_a of 3.44 [120]. The titration curve of a defective sample of UiO-66 reveals three apparent inflection points at pH 5.44, 7.56 and 9.51, corresponding to pK_a values of 3.52, 6.79 and 8.30, respectively (Figure 18). The lowest pK_a was assigned to the μ_3-OH groups, in agreement with the observation made for UiO-67. The authors tentatively assigned the remaining pK_a values to the Zr–OH_2 (6.79) and Zr–OH (8.30) protons present as compensating

species at defective sites. Similar results were obtained upon titration of the eight-connected NU-1000 (calculated pK_as of 3.59, 5.75 and 8.2) and six-connected MOF-808 (calculated pK_as of 3.64, 6.22, 8.23 and 9.12; the fourth titratable proton was not assigned in this case). Based on this study, the authors speculated that Zr-MOFs could also be active in acid-catalysed reactions and investigated whether there is any correlation between the number of defects and their activity towards promotion of the epoxide ring-opening reaction with an alcohol (Scheme 1) [121]. In fact, they found that the catalytic activity is a direct function of the number of defects, with MOF-808 being the best performing material, in agreement with its status of more defective compound.

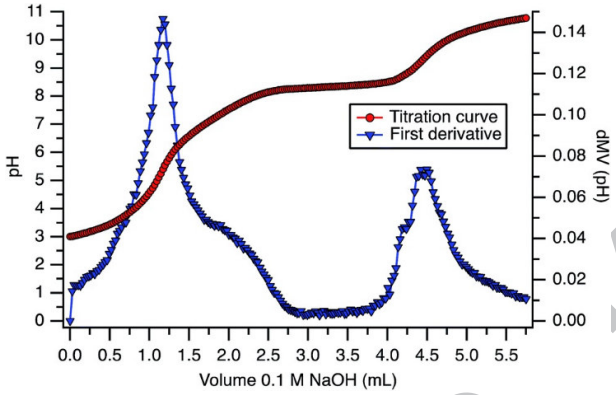

Figure 18. Titration curve of a defective UiO-66 sample (red) and corresponding first derivative (blue), showing three equivalent points at pH 5.44, 7.56 and 9.51. [Reprinted with permission from ref. [120]. Copyright 2016, Royal Society of Chemistry.]

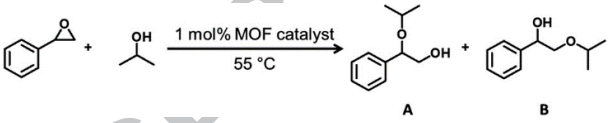

Scheme 1. Styrene-oxide ring-opening reaction with isopropanol catalysed by Brønsted acidic defective Zr-MOFs. [Reprinted with permission from ref. [121]. Copyright 2016, Royal Society of Chemistry.]

Defects were also harnessed to improve proton conduction in UiO-66, taking advantage of the increase in both pore volume and number of acidic sites upon creation of defects, with the aim of enhancing mobility of the charge carrier [122]. Defective samples were prepared either by using substoichiometric amounts of linker or by adding a modulator during the synthesis [AA or stearic acid (SA, Chart 2)]. For the series of non-modulated samples, proton conductivity increases by about two orders of magnitude when the amount of missing linkers increases from 5% to 23%, as a result

of the presence of more Zr-OH and Zr-OH_2 Brønsted acid sites (Figure 19). When AA is included as a compensating group in place of hydroxide and water, conductivity is the same as the least defective non-modulated sample. This suggests that the sole increase of pore volume is not enough to enhance proton mobility. The materials produced using SA as a modulator prove to be the most effective ones, because SA is effective in competing with bdc^{2-} to create defects, but cannot be incorporated in the MOF due to its sterically demanding alkyl chain. As a result, UiO-66 featuring both larger pore volume and higher density of Brønsted acid sites was obtained, yielding a remarkable proton conductivity of 6.93×10^{-3} S cm^{-1} at 65 °C and 95% relative humidity (RH).

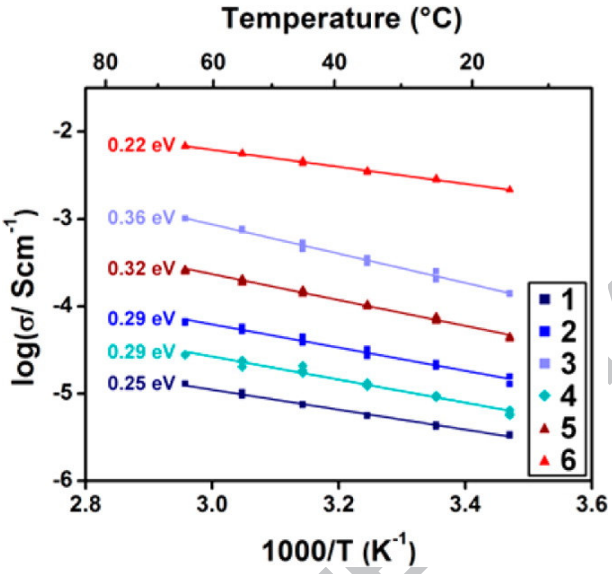

Figure 19. Proton conductivity measured from alternate current (AC) impedance analysis, with corresponding activation energies, for non-modulated UiO-66 samples containing 5% (**1**, dark blue), 13% (**2**, blue) and 25% of missing-linker defects (**3**, light blue), for an AA-modulated UiO-66 sample (**4**, teal) and for SA-modulated UiO-66 samples having 7% (5, dark red) and 17% of missing-linker defects (**6**, red). [Reprinted with permission from ref. [122]. Copyright 2015, American Chemical Society.]

4. Controversies and open issues

4.1 Missing-linker versus missing-cluster

The central unresolved issue concerning defects in Zr-MOFs is the missing-linker/missing-cluster dichotomy. Although a brief and objective account about the discovery of missing-linker and missing-cluster defects has been given in Section 2, the present subsection is intended to critically address the topic.

Missing-linker defects were initially deemed responsible for the deviations from the ideal behaviour evidenced by TGA and nitrogen sorption analysis in defective samples of UiO-66 [90, 91]. This hypothesis is based on the observation that samples exhibiting a smaller weight loss at 450 °C display an increase of surface area, suggesting that defects have to be localized in the organic part of the framework. Early crystallographic studies corroborated the hypothesis, showing that defective samples can indeed be modelled by assuming that linkers are randomly removed throughout the face-centered cubic crystal structure and refining the occupation factors of the carbon atoms constituting them [61, 91, 94]. The discovery of missing-cluster defects brought to attention the fact that defects can actually affect also the inorganic part of the framework and can be generated in an ordered fashion [92]. Similar to missing linkers, missing-cluster defects lead to an overall deficiency of organic matter in the framework and to an increase of surface area if compared to defect-free UiO-66, suggesting the two types of defects could not be effectively distinguished on the basis of TGA and nitrogen sorption analysis. However, the presence of missing clusters is normally thought to be unambiguously revealed by the appearance of weak superlattice reflections in the diffraction pattern, because of their tendency to cluster in correlated nanodomains.

After the discovery of missing-cluster defects, people assumed that the formation of missing linkers and missing clusters could be dependent on the synthetic conditions and that they could even coexist in the same crystal. This dualism was recently questioned, proposing that missing-cluster defects might actually be the only type of defects existing in UiO-66 [93]. This conclusion is grounded on the comparison between simulated and experimental nitrogen adsorption isotherms. UiO-66 was prepared using a range of modulators with different acidity (FA, AA, DFA and TFA) and it was noticed that the calculated isotherms for model structures incorporating random missing-linker defects cannot match the experimental ones, especially when DFA and TFA were used as modulators (Figure 20, left and right graphs). Structural models with pure **reo** topology and monocarboxylates as compensating groups were then generated and it was found that the simulated adsorption isotherms well describe the experimental isotherms obtained for the most defective samples, i.e. those synthesized in the presence of 36 equivalents of either DFA or TFA (Figure 20, center and right graphs). This suggests that these samples contain such a high concentration of missing-cluster defects that their crystal structure has basically full **reo** character. However, their PXRD patterns display the usual sharp reflections associated with the **fcu** phase and only a very broad peak in correspondence of the calculated positions of the (100) and (110) reflections associated with the **reo** phase (Figure 21). While this behaviour could be reasonable for samples having low defectivity, it does not seem to be realistic for highly defective ones. Although the intensity of the broad peak appears to be correlated with the defectivity of the MOFs, one would expect the PXRD patterns to

display a single set of reflections having the same line shape associated with the *Pm*-3*m* unit cell. The authors tried to explain this incongruence hypothesising that the crystalline domains are very small, but did not dig deeper into this issue. Pore size distribution analysis could have provided further support to prove the authors' point, because it should have clearly displayed a massive presence of pores having size in the 16-18 Å range associated with the **reo** framework, but unfortunately it was not performed.

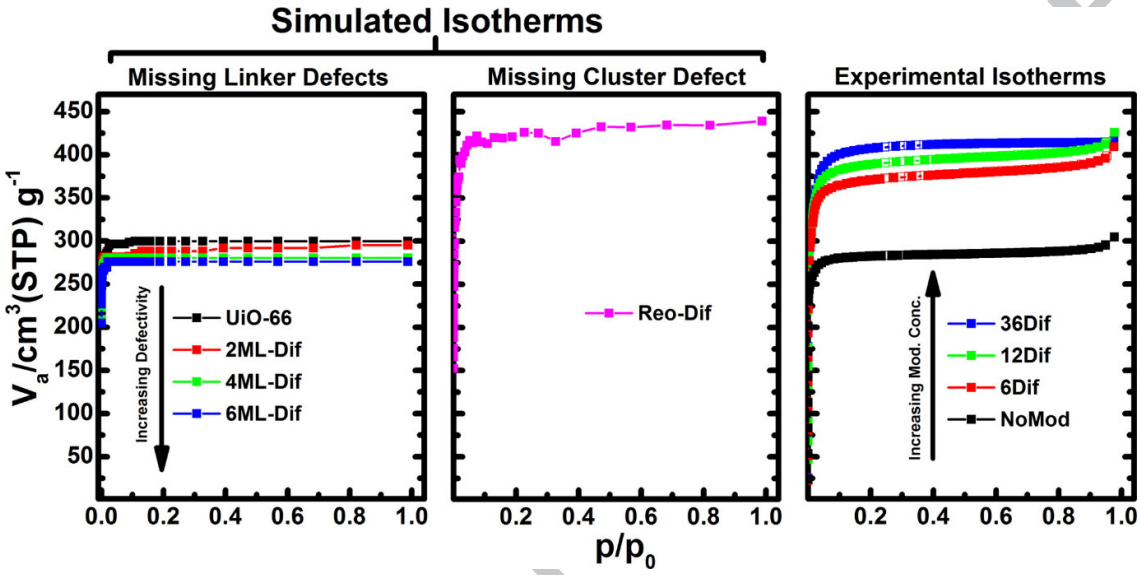

Figure 20. Comparison of experimental nitrogen sorption isotherms for a non-modulated (black) and DFA-modulated UiO-66 samples (6 equivalents, red; 12 equivalents, green; 36 equivalents, blue) (right) with simulated isotherms obtained from models incorporating 0 (black), 2 (red), 4 (green) and 6 (blue) missing linkers per unit cell (left) and from a pure **reo** framework (centre) containing DFA as a terminal ligand. [Reprinted with permission from ref. [93]. Copyright 2016, American Chemical Society.]

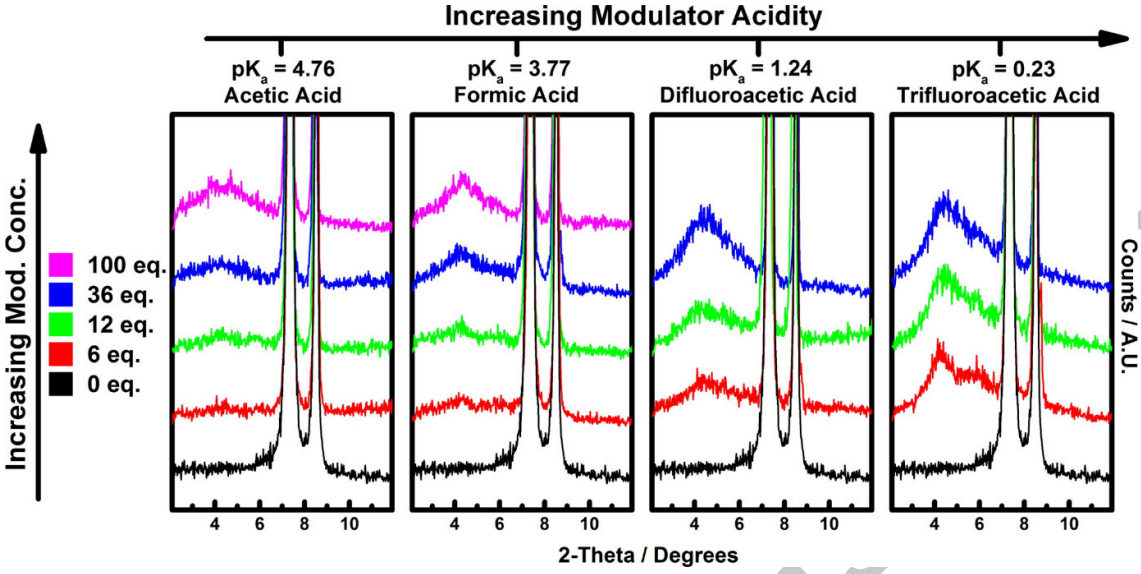

Figure 21. PXRD patterns of solvent-evacuated UiO-66 samples prepared using monocarboxylic acids having different acidity as modulators. From left to right: AA, FA, DFA, TFA. Syntheses using 100 equivalents of either DFA or TFA gave no MOF product. [Reprinted with permission from ref. [93]. Copyright 2016, American Chemical Society.]

The preference towards the ordered formation of defects finds theoretical backing in a paper published almost simultaneously [123]. The authors calculated the free energy of defect formation for all the possible configurations associated with removal of one to three linkers from the unit cell. It turns out that when more missing-linker defects are introduced in the unit cell, the configurations where the defects are generated in a more ordered fashion are by far the most energetically favourable. Even more striking is the scenario where a defective structure featuring eight missing-linker defects created in a symmetric fashion, matching the node structure of NU-1000, was tested, finding that the energy associated with the formation of this structure is similar to the cost of a single missing-linker defect (Figure 22).

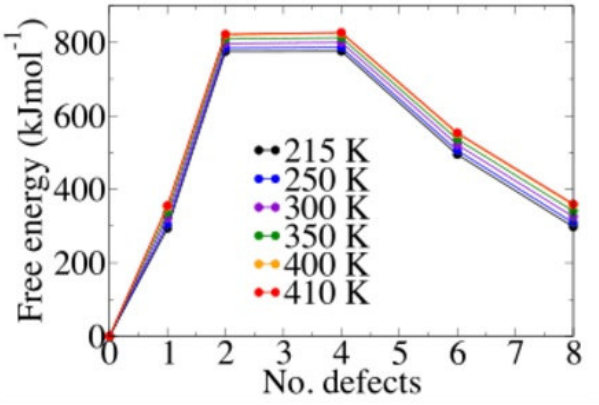

Figure 22. Reaction energy at different temperatures for removing one, two, four, six and eight linkers in an ordered fashion from UiO-66 with OH^-/H_2O as compensating species. [Reprinted from ref. [123]. Copyright 2016, American Chemical Society.]

The cost of removal of one cluster and twelve linkers to yield the **reo** structure was not investigated, although in retrospect it would be of extreme interest to help unravelling the missing-linker/missing-cluster dualism. In another article [92], it was calculated that the **reo** phase is less stable by 61.8 kJ mol(Zr)$^{-1}$ than the **fcu** phase, but this number cannot be straightforwardly compared to those obtained in ref. [123]. The superior mechanical stability of the **reo** structure with respect to a model where four linkers per cluster are randomly removed from the **fcu** framework, evidenced in ref. [103] seems to point in the same direction of favouring order over randomness, but it is clear that further investigation is needed to produce a definitive proof of the model featuring exclusively missing-cluster defects.

4.2 Nature of the compensating species

Together with the missing linker/missing cluster dualism, one of the most debated topics regarding defects in Zr-MOFs is the nature of the species present at defective sites to fill coordination vacancies on the metal atoms and to ensure electroneutrality. Looking back into the present review, the reader might have noticed that several different models, sometimes in apparent conflict with each other, were proposed. Both experimental evidences and theoretical calculations were invoked in support of a given model, but a clear understanding of this aspect is still lacking.

It is straightforward that the reaction environment in which the MOF is generated determines which species will end up being incorporated at defective sites. Nonetheless, even in the simplest system consisting of a zirconium source (typically $ZrCl_4$ or $ZrOCl_2{\cdot}8H_2O$), an organic linker, water and DMF, there are several species that could compete for coordination to defective clusters. Being negatively charged, OH^- and Cl^- can both fill the coordination vacancies and compensate the excess positive

charge. Besides them, H_2O and DMF could coordinate to Zr atoms and eventually be retained in the crystal structure. It has to be remarked that the presence of H_2O and DMF alone would not compensate the charge excess, therefore they could be incorporated only as "ancillary" groups alongside anionic species. In addition, DMF can undergo hydrolysis to form dimethylamine and FA [95, 124], which can bind to Zr clusters as well. Addition of concentrated HCl as a protonation modulator does not increase the number of species competing for the defective sites, but it influences several reaction parameters by increasing the acidity of the reaction medium and, in turn, the availability of OH^- and the hydrolysis rate of DMF [125]. Further complexity is introduced in the system upon addition of monocarboxylic acids as coordination modulators, sometimes in combination with HCl. In one isolated case, HF was also used to modulate the synthesis [63]. Table 2 summarizes all the different scenarios proposed so far on the basis of experimental observations.

Table 2. Relevant examples of experimentally observed compensating groups in defective Zr-MOFs prepared using a range of modulators.

Zr-MOF	Modulator	Compensating group	Reference
UiO-66	HCl	OH^-/H_2O	[62]
UiO-66	AA	AA	[91]
UiO-66	TFA + HCl	TFA	[112]
UiO-66	HCl	Cl^-	[95]
UiO-66	BA	OH^-/H_2O/DMF	[61]
UiO-66	FA	H_2O + extra-framework OH^- or PrO^-	[94]
UiO-66	HCl	OH^-/H_2O	[115]

UiO-66	HF	F^-	[63]
UiO-66	TFA	TFA	[104]
UiO-66	FA; AA; DFA; TFA	FA; AA; DFA; TFA	[93]
UiO-66	BA	BA	[126]
UiO-66	HCl; FA	Cl^-; FA	[46]
UiO-66	BA	BA	[127]
UiO-66	none; AA; SA	OH^-; AA; OH^-	[122]
UiO-66(Hf)	FA	FA	[99]
UiO-66(Hf)	FA	FA	[92]
UiO-66/UiO-67	FA; AA; BA; TFA	FA; AA; DFA; TFA	[128]
UiO-66/UiO-67	HCl	OH^-/H_2O	[120]
UiO-66/UiO-67	HCl	OH^-/H_2O	[121]
UiO-66/UiO-67/Zr-muconate	Gly + HCl; *L*-Pro + HCl; *L*-Phe + HCl	Gly; *L*-Pro; *L*-Phe	[59]
DUT-52	*L*-Pro	*L*-Pro	[58]
MOF-808	FA	FA	[4]
MOF-808	FA; AA; PA	FA; AA, PA	[96]
NU-1000	BA	BA	[3]
DUT-51	BA	BA	[6]
DUT-53	AA	AA	[64]
DUT-84	AA	AA	[64]

Investigating the synthesis of UiO-66 from a $ZrCl_4/H_2bdc$/conc. HCl/DMF reaction mixture, it was observed that IR spectra of defective samples display more peaks in the O–H stretching region than the material prepared without addition of HCl, concluding that OH^- and H_2O are the most abundant compensating species [62]. Elemental analysis indicates that only 10% of the vacant sites contain Cl^-. Shortly thereafter, the same authors demonstrated that OH^- and H_2O groups in defective UiO-66 prepared with the same procedure can in fact be distinguished and quantified by acid-base titration [120]. Other works from the same group assumed the same type of model, justified by experimental observations [115, 121]. A definitive molecular-level characterization of the coordination environment around the defective clusters from SCXRD data was claimed to have been achieved [94]. In the proposed model, two water molecules coordinate to the zirconium atoms at defective sites and electroneutrality of the system is guaranteed by the presence of extra-framework

hydroxide anions hydrogen-bonded to the -OH groups in the clusters (Figure 23). These -OH species are still present after treatment of the crystal at 500 K under vacuum, which leads to removal of the coordinated water molecules, suggesting that they are strongly bonded to the clusters. When zirconium propoxide is used as a starting material for the synthesis, propoxide anions replace the hydroxide anions. The presence of formate (used as modulator) or halogenides (present in the reaction environment when $ZrCl_4$, $ZrOCl_2 \cdot 8H_2O$ or $ZrBr_4$ were employed as starting materials) was ruled out. However, this model was successively contradicted by two independent theoretical studies [129, 130], which demonstrated that the predicted most stable configuration is actually the one where one OH^- and one H_2O are coordinated to the cluster and one H_2O is held in their proximity by hydrogen-bonds (Figure 24).

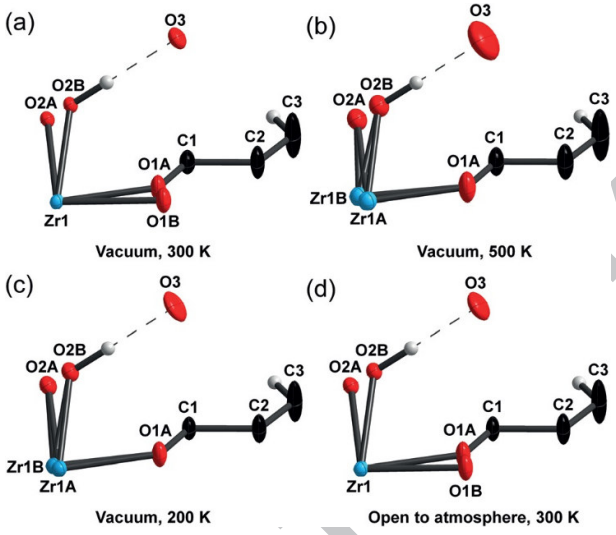

Figure 23. Asymmetric unit of defective UiO-66 measured at room temperature under vacuum (**a**), heated to 500 K, with loss of coordinated water molecules (O1B) (**b**), cooled to 200 K (**c**) and warmed back to room temperature and exposed to the atmosphere, where the water molecules are once again coordinated to Zr (**d**). Colour code: Zr, light blue; O, red; C, black; H, white. Ellipsoids are shown at 50% probability. [Reprinted with permission from ref. [94]. Copyright 2015, John Wiley and Sons, Inc.]

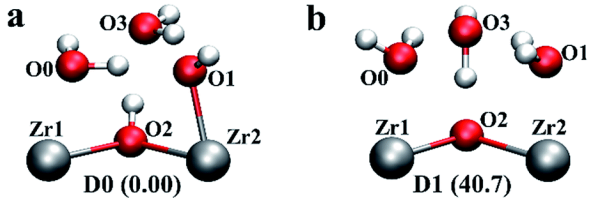

Figure 24. Computationally generated local geometries for defective clusters in UiO-66: one OH^- (O1) and one H_2O (O0) coordinated to Zr, with one hydrogen-bonded H_2O (O3) and a μ_3-OH group (O2)

(configuration D0; **a**); two H_2O coordinated to Zr, with one hydrogen-bonded H_2O and a μ_3-O group (configuration D1, similar to that proposed in ref. [94]; **b**). The relative energies in kJ mol^{-1} are given in brackets with respect to defect configuration D0. Colour code: Zr, silver; O, red; H, white. [Reprinted from ref. [129]. Copyright 2016, Royal Society of Chemistry.]

Further ambiguity was created when the presence of H_2O/OH^- in UiO-66 obtained in the presence of HCl as a modulator was excluded based on diffuse reflectance infrared Fourier transform spectroscopy (DRIFTS), which shows no other O-H stretching bands than that of the μ_3-OH groups in the clusters [95]. Formate was not observed in the NMR spectrum of the dissolved samples and was ruled out as well. Energy dispersive X-ray spectroscopy (EDS) reveals the presence of Cl^- in all the defective samples, suggesting that this is the compensating species. In another work, EDS shows that Cl^- is also present in a non-modulated defective sample [63], but it is completely replaced by F^- when HF is used as a modulator in small amounts (1 to 3 equivalents). This is due to the high affinity between zirconium and F^-, which can be incorporated in the crystal structure even when it is used as a modulator in the presence of strong ligands such as phosphonates [131-134]. A theoretical contribution to the debate came by the calculation of the free energies of defect formation for different combinations of compensating groups [123]. The authors found that the order of stability between 225 and 400 K is $Cl^-/H_2O \geq Cl^- > Cl^-/DMF >> OH^-/H_2O > OH^- > OH^-/DMF$, suggesting that the incorporation of Cl^- is always favoured over OH^-, irrespective of the presence and nature of the neutral ancillary group.

When monocarboxylic acids are employed as modulators, there is much better agreement among different studies: the respective conjugate anions are found to be preferentially incorporated as compensating groups, even when HCl is also added to the reaction mixture. Monocarboxylic modulators are necessary for the synthesis of intrinsically defective Zr-MOFs, such as MOF-808 [4], NU-1000 [3], DUT-51 [6], DUT-53 and DUT-84 [64]. As a consequence of the long-range crystallographic order existing in these materials, incorporation of monocarboxylates in the clusters occurs in an ordered fashion. Two computational studies confirmed that structures featuring TFA or AA at defective sites are energetically easier to access than those where either Cl^- or OH^- bind to the clusters [113, 123]. However, two remarkable exceptions were reported: i) no electron density compatible with benzoate groups coordinated to the clusters was observed in single crystals of UiO-66 prepared in the presence of BA [61], although in a subsequent work the same group contradicted this claim based on the detection of BA by NMR after dissolution of the MOF [126]; and ii) similarly, the presence of formate in single crystals of UiO-66 obtained using FA as a modulator was excluded [94]. Despite being in sharp contrast with the rest of the literature, these papers cannot be

overlooked, because they report detailed crystal structures obtained from SCXRD data. The case reported in ref. [122], where stearate cannot comprehensibly be incorporated due to its sterically demanding 18-membered alkyl chain, is self-standing and cannot be considered as a relevant exception.

4.3 Post-synthetic modification of defects

PSM methods have been largely explored, proving to be a very useful tool for functionalization of the framework of Zr-MOFs [76]. In particular, direct exchange of linkers in the framework of Zr-MOFs can be easily performed with the aid of a solvent, a process termed post-synthetic exchange (PSE) [80, 83]. Even materials that cannot be obtained using other synthetic methods have been prepared *via* PSE [20, 29, 81, 82]. A few recent papers suggest that the presence of defects offers additional opportunities for performing post-synthetic modification of Zr-MOFs *via* exchange of compensating groups grafted at defective sites.

When PCN-222 [based on the tetrakis(4-carboxyphenyl)porphyrin ($tcpp^{4-}$, Chart 1) linker and eight-connected clusters] was synthesized in the presence of BA as a modulator, the authors treated the MOF with HCl/DMF in order for its measured porosity to reach the value calculated on the basis of the crystal structure [5]. The same approach was applied on the similar NU-1000 and NMR analysis of the dissolved materials shows that the signals related to BA disappear after activation. This proved that the activation procedure is necessary to remove benzoate groups coordinated to the clusters of the as-synthesized MOF and to replace them with OH^- and H_2O. [3]. This observation inspired the development of an approach termed “solvent assisted ligand incorporation” (SALI) to functionalize the defective sites of the eight-connected clusters of NU-1000 with a range of monocarboxylates [135, 136].

It was later demonstrated that monocarboxylate groups grafted at defective sites in UiO-66 and UiO-67 can be post-synthetically exchanged with other monocarboxylic species in a SALI-like fashion, by simple soaking of the MOF in a solution of the desired acid (Figure 25) [128]. The same happens also on HCl-modulated samples contacted with organic acids and on organic acid-modulated samples contacted with HCl, demonstrating the versatility of the method. The authors also claimed to have “healed” a defective sample of BA-modulated UiO-67 by soaking it in a solution of $bpdc^{2-}$, as proved by the absence of BA signals in the NMR of the dissolved MOF and by the decrease of surface area upon defect healing. In addition, the healed MOF does not show appreciable uptake of AA. FA- and AA-modulated UiO-67 subject to the same treatment also uptake $bpdc^{2-}$ and release FA and AA, but they undergo further exchange when contacted with a solution of AA. The authors speculated that the different behaviours are the result of different types of defects: the BA-modulated sample

contains mainly missing-linker defects, allowing irreversible installation of the bridging linkers, whereas the FA- and AA-modulated MOFs contain missing-cluster defects, allowing $bpdc^{2-}$ to coordinate through only one carboxylic group and to be incorporated in a reversible fashion.

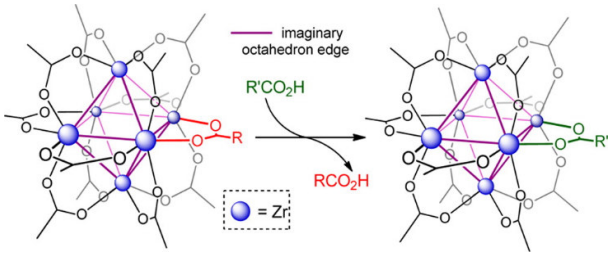

Figure 25. Pictorial representation of SALI-like process on a UiO-66-type defective Zr-MOF. [Reprinted with permission from ref. [128]. Copyright 2015, American Chemical Society.]

Sequential linker installation (SLI) is an elegant example of a procedure similar to defect healing involving missing-linker defects [137]. The authors took advantage of the eight-connected clusters in PCN-700 [based on 2,2'-dimethylbiphenyl-4,4'-dicarboxylate (Me_2-$bpdc^{2-}$, Chart 1) as a linker] to perform SLI (Figure 26). They noticed that the structure of PCN-700 features two different types of pockets in between adjacent clusters that could ideally accommodate bridging linkers of appropriate size. In fact, they demonstrated that bdc^{2-} and 2',5'-dimethylterphenyl-4,4''-dicarboxylate (Me_2-$tpdc^{2-}$, Chart 1) can be post-synthetically installed onto the defective sites of PCN-700, giving rise to a range of mixed-linker Zr-MOFs. The scope of the SLI approach was later expanded, proving its effectiveness for tailoring of pore size and shape and flexibility [138, 139].

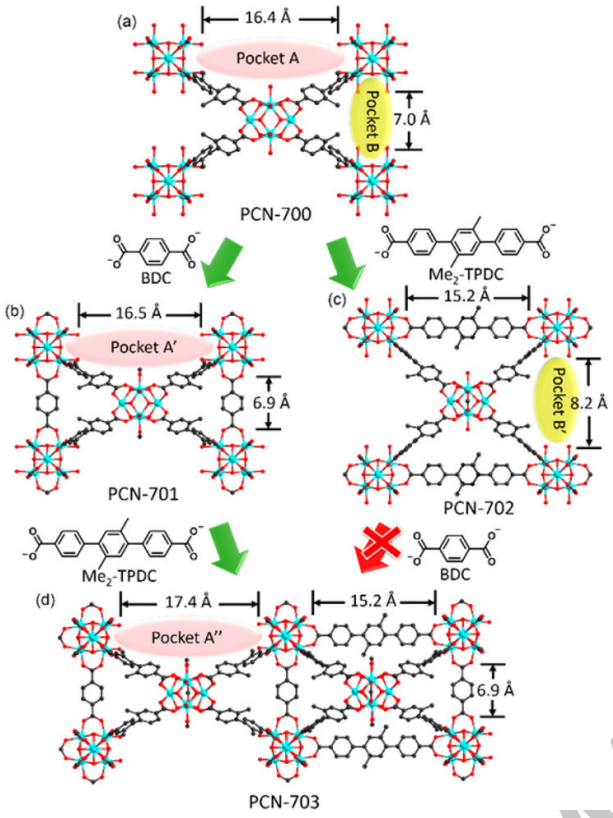

Figure 26. PCN-700 (**a**) features two pockets having different size: 16.4 Å (Pocket A) and 7.0 Å (Pocket B). Installation of bdc^{2-} in Pocket B of PCN-700 leads to PCN-701 (**b**), slightly increasing the size of Pocket A to 16.5 Å (Pocket A'). Me_2-$tpdc^{2-}$ is installed in half of Pockets A', reducing the size to 15.2 Å and leading to PCN-703 (**d**), which features open enlarged Pocket A'' (17.4 Å). Installation of Me_2-$tpdc^{2-}$ in the Pocket A of PCN-700 leads to PCN-702 (**c**), increasing the size of Pocket B to 8.2 Å (Pocket B') and preventing installation of bdc^{2-}. Colour code: Zr, light blue; O, red; C, dark grey. [Reprinted with permission from ref. [137]. Copyright 2015, American Chemical Society.]

The above-mentioned articles highlight the dynamic nature of defects, demonstrating how compensating groups at defective sites can readily be exchanged, reproducing at the solid state what has been observed in solution for clusters decorated exclusively with monocarboxylate groups [140-142]. This is not very surprising, if one considers that even bridging dicarboxylates can be displaced with relative ease by other bridging linkers having analogous size and geometry during PSE [80]. More intriguing are the manifold implications of the possible involvement of defects in post-synthetic manipulation. Two different scenarios can be envisioned, depending on whether missing-linker or missing-cluster defects are concerned. In the case of missing linkers (Figure 27), post-synthetic defect healing (PSDH) should be possible upon replacement of two monocarboxylates with one dicarboxylate, as suggested in ref. [128] (Figure 27, **a** to **b**). The reverse phenomenon, which can

be termed post-synthetic defect generation (PSDG), might as well occur in appropriate reaction conditions (although not yet reported) (Figure 27, **b** to **a**). During PSE, the new linker would be installed in place of another dicarboxylate, leaving the defective site unchanged (Figure 27, **a** to **c**). However, it is more likely that PSE and PSDH would compete, although proceeding with different kinetics depending on whether the species to be exchanged are two monocarboxylates or one dicarboxylate. This might eventually lead to decreased defectivity of the PSE'd MOF compared to the pristine MOF, if both the processes took place on comparable time scales (Figure 27, **a** to **d**).

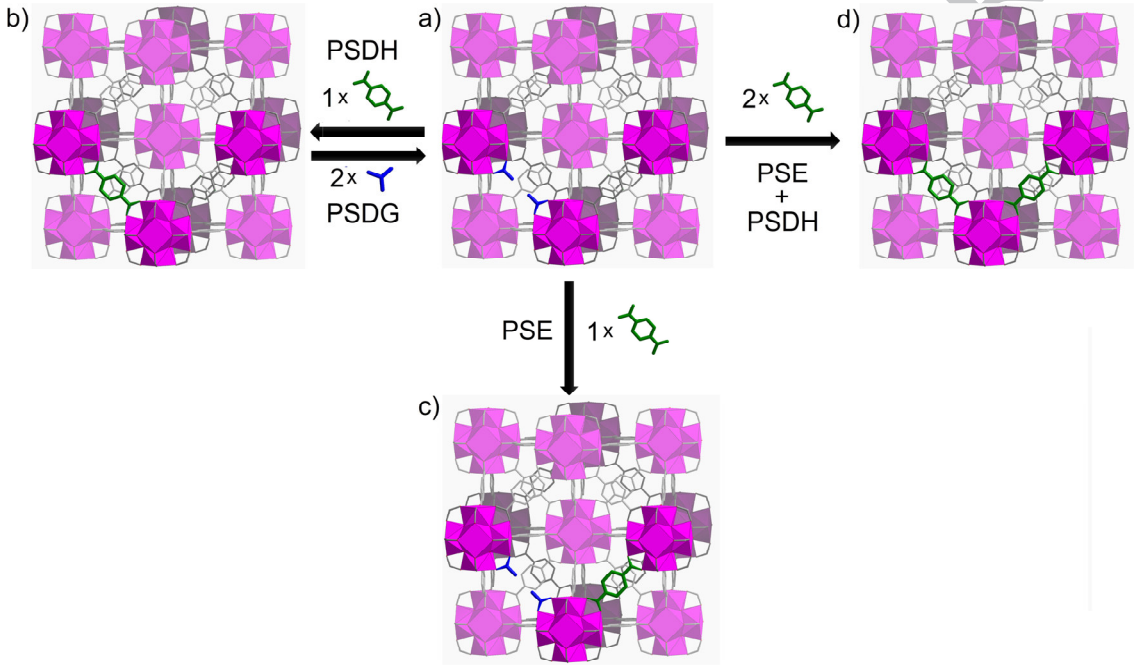

Figure 27. Possible post-synthetic defect modifications in a missing-linker scenario: a unit cell featuring one missing linker (**a**) can undergo reversible PSDH/PSDG (**b**), PSE (**c**), or combined PSE and PSDH (**d**). Colour code: ZrO_8 polyhedra, pink; O, red; C, grey; exchanged linker, green; monocarboxylic compensating group, blue. H atoms are omitted. For the sake of clarity, the clusters which do not undergo any change are shaded.

If missing clusters are considered, the situation is very different and more intricate. In order to perform PSDH, the defective MOF should be soaked in a solution containing both the linker and the metal, and $[Zr_6O_4(OH)_4(L)_{12}]^{12-}$ units should substitute twelve monocarboxylates grafted at defective sites (Figure 28, **a** to **b**). This seems to be highly unlikely, since these units should have a strong tendency to polymerize and a few monomers should be available in solution. PSDG could in principle be possible, but it would also be highly improbable, because it would require the introduction of twelve monocarboxylates in an extremely ordered fashion to allow a $[Zr_6O_4(OH)_4(L)_{12}]^{12-}$ unit to be

released (Figure 28, **b** to **a**). Soaking of the defective MOF in a solution of a dicarboxylic linker could result in two distinct processes: i) reversible displacement of terminal monocarboxylates, a process already observed [128] that can be termed post-synthetic defect exchange (PSDE) (Figure 28, **a** to **c**); or ii) PSE, without involving the defective sites (Figure 28, **a** to **d**). Similar to the missing-linker case, the two processes of PSDE and PSE would likely be competitive and could even occur simultaneously (Figure 28, **a** to **e**). However, part of the newly installed dicarboxylates upon PSE-PSDE would be prone to undergo further PSDE, being easily displaced in a successive treatment with monocarboxylic acids (Figure 28, **e** to **d**).

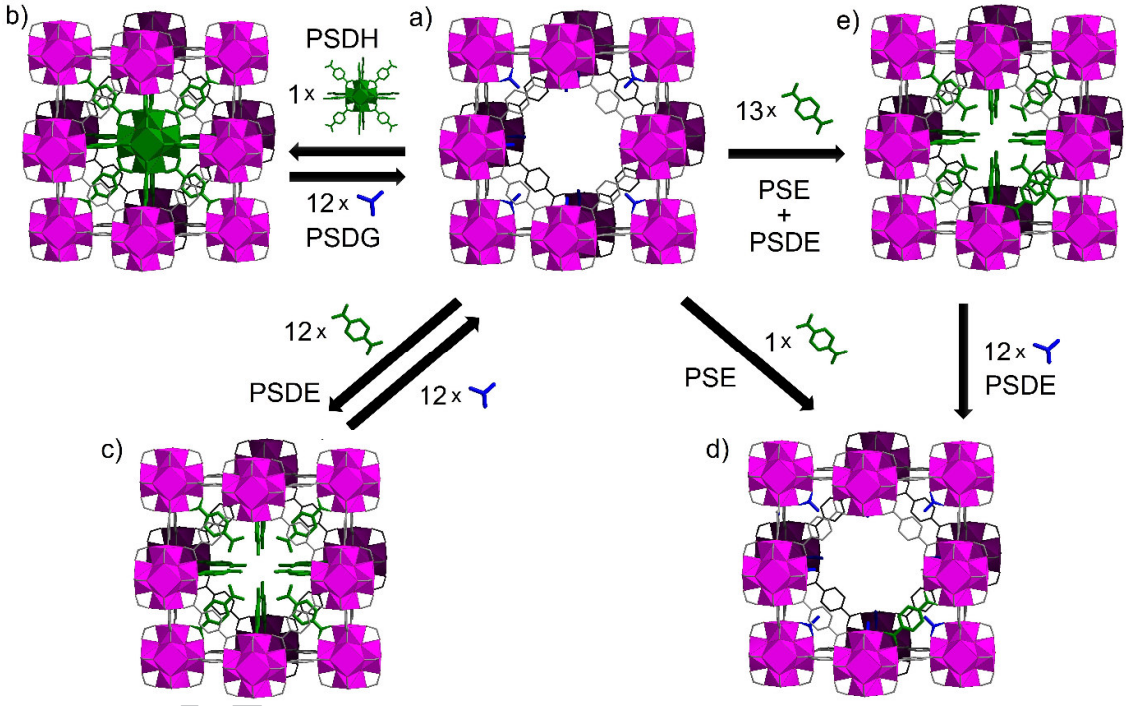

Figure 28. Possible post-synthetic defect modifications in a missing-cluster scenario: a unit cell featuring one missing cluster (**a**) can undergo PSDH/PSDG (**b**), reversible PSDE (**c**), PSE (**d**) or combined PSE/PSDE (**e**). (**e**) can undergo further PSDE leading to (**d**). Colour code: ZrO_8 polyhedra, pink; O, red; C, grey; exchanged linker, green; monocarboxylic compensating group, blue. H atoms are omitted.

Besides the potential for framework functionalization, which is discussed in the outlook, the interest in understanding the role of defects in PSM is also related to the useful information that can potentially be gathered to address the missing linker/missing cluster dualism, contributing to draw a clearer picture of defects in Zr-MOFs. Little insight into these aspects has been gained so far and there is plenty of room for further investigation.

4.4 Effect of linker functionalization on defects

Most of the studies about defects in UiO-66 were carried out on the pristine material based on bare bdc^{2-} linkers, most likely assuming that using functionalized linkers would result in isoreticular structures with no significant influence on defects. However, the case of the Zr-MOF based on 2-sulfoterephthalic acid (H_3sbdc, Chart 1) stands out as a remarkable exception. This material was first synthesized in 2013 and its PXRD pattern was indexed with a body-centred cubic unit cell having space group *Im*-3 and unit cell parameter (41.490 Å), twice as large as the one of UiO-66 (20.700 Å), suggesting that the two structures are related [143]. Soon thereafter, a different group succeeded in solving the crystal structure of Zr-sulfoterephthalate, finding that it can be considered as a unique ordered defective version of UiO-66 where six out of eight clusters ideally sitting on the corners of the UiO-66 unit cell are missing along with their linkers (Figure 29) [144]. As a consequence, the framework is based on both twelve-connected and nine-connected clusters and large pores are present, in addition to the usual tetrahedral and octahedral cages found in UiO-66. The authors speculated that the formation of such an unusual defective structure could be the result of both highly acidic conditions during synthesis and the steric bulk of the sulfonate group. The case of Zr-sulfoterephthalate is an extreme (and so far unique) example of the influence that functionalized linkers can exert on the defectivity of a Zr-MOF. Although it is possible that other functional groups are not able to determine the formation of a similar ordered defective structure, their acid/base, steric, electronic and symmetric features could play a role in either promoting or hindering defect generation that has not yet been object of systematic investigation.

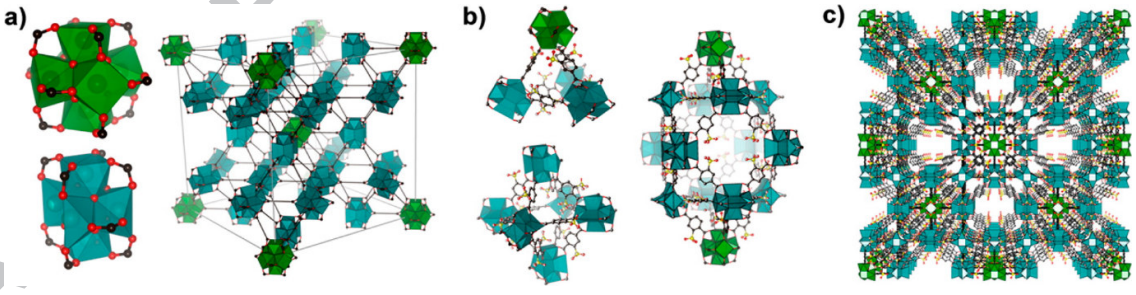

Figure 29. Polyhedral representation of the Zr clusters and their connectivity in the unit cell of Zr-sulfoterephthalate (**a**), structure of tetrahedral and octahedral cages and large pore (**b**) and view of a 2 × 2 × 2 unit-cell model (**c**), highlighting the presence of channel-like pores. Colour code: 12-connected clusters, green; 9-connected clusters, teal; O, red; C, black; S, yellow. [Reprinted with permission from ref. [144]. Copyright 2015, American Chemical Society.]

4.5 Unravelling the crystallization mechanism

The literature concerning Zr-MOFs is growing at an impressive rate, but a significant gap of knowledge about their crystallization mechanism still exists, if compared with other benchmark MOFs, such as MIL-101 [145-148], MIL-100 [149, 150], MIL-53 [147, 151], ZIF-8 [152-155], HKUST-1 [156-158], MOF-5 [159-164]. *In-situ* methods have been crucial to investigate the crystallization of these MOFs [165]. Understanding how Zr-MOFs are formed from their building blocks would allow the fine-tuning of their features, including defects, in a rational manner.

Two *in-situ* PXRD studies evidenced the influence of water and monocarboxylic modulators on the crystallization kinetics of UiO-66 [166] and Zr-fumarate [167], respectively. The main outcomes of these two studies are: i) nucleation is the rate-determining step; ii) water accelerates the formation of Zr-MOFs by enhancing nucleation, presumably by favoring hydrolysis of the Zr precursor; iii) monocarboxylic acids slow down nucleation, most likely by competing with the linkers for coordination to the metal, thus allowing the growth of large crystallites. However, no real mechanistic insight was gained and the conclusions drawn about the role of water and modulators are based on common chemical sense. No intermediate crystalline phases were observed during *in-situ* monitoring of the reaction. A remarkable step forward was recently made by following crystallization by *in-situ* small and wide angle X-ray scattering (SAXS and WAXS, respectively) and developing a DFT-based metal-organic molecular orbital (MOMO) analysis to investigate the self-assembly process [168]. The authors discovered that the formation of UiO-66 crystals occurs upon deprotonation of an amorphous metastable proto-UiO-66 phase containing superprotonated $[Zr_6(OH)_8]^{16+}$ clusters already interconnected *via* the bdc^{2-} linkers (Figure 30). The protons released during the final step that leads to crystalline UiO-66 favour the condensation of clusters and linker to form the metastable phase, resulting in an autocatalytic process in which crystallization accelerates as it progresses. These findings provided an explanation for the acceleration in the formation of UiO-66 and UiO-67 upon addition of HCl to the reaction mixture, first observed in 2013 [62].

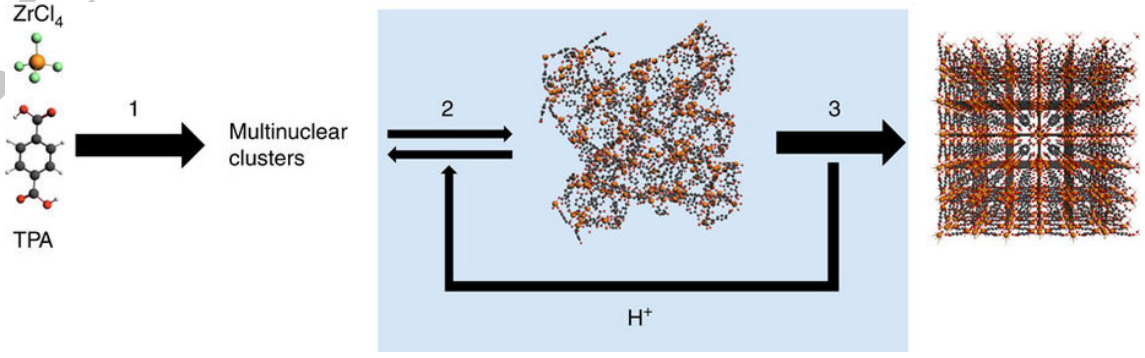

Figure 30. Proposed mechanism of crystallization for UiO-66: formation of multinuclear clusters from $ZrCl_4$ and H_2bdc (named TPA in the figure) (step 1); consumption of H^+ and fast condensation into an amorphous metastable proto-UiO-66 phase (step 2); development of crystallinity upon release of H^+ (step 3). [Reprinted from ref. [168]. Copyright 2016, Nature Publishing Group.]

Despite the recent advances, we are still far from having a detailed enough picture of the crystallization mechanism that could account for the huge pool of experimental evidences collected so far, along with their related contradictions. The pathway of formation of $Zr_6O_4(OH)_4(COO)_{12}$ SBUs from the Zr precursor, water and the organic linkers still remains unknown, despite being a key step during the assembly of the framework, which ultimately inherits the symmetric features of the parent SBU [169, 170]. This lack of understanding can be ascribed to the complexity of the chemistry taking place during crystallization, where DMF can also play a major role in the process of SBU formation, as already demonstrated for other MOFs [147, 171, 172], by virtue of its coordinative character. As a matter of fact, several zirconium complexes featuring DMF as a ligand are known to exist [173-176]. A contribution might come from the mechanistic studies previously carried out on molecular clusters [141, 177, 178], although these are usually synthesized in rather different conditions and are soluble in many solvents, which makes them much easier to be characterized *in-situ*. The **reo**-**fcu** relationship is another relevant open question: it is known that the **reo** defective phase is favoured at low synthesis temperatures [95, 179], and in the presence of large amounts of monocarboxylic modulators [93], suggesting that it is a kinetic product. However, it is still unclear whether the **reo** phase is the product of an independent reaction path or a metastable intermediate phase towards the formation of the thermodynamically favoured **fcu** phase.

5. Outlook

The fundamental (and controversial) aspects highlighted in the previous section need to be addressed in the near future in order to gain a deep understanding of the very nature of defects in Zr-MOFs. However, it is clear that these defects can be harnessed and turned into virtues, offering a range of brand new opportunities for tailoring the properties of Zr-MOFs. Special attention will likely be drawn by UiO-66, which is the prototypical Zr-MOF and remains by far the most investigated for prospective applications on a large scale, being based on the readily available and inexpensive H_2bdc linker. The scenario in which missing clusters are the dominant type of defects existing in UiO-66 [93], at least when monocarboxylic acids are used as modulators, is extremely fascinating for expanding the scope of this material for applications.

A defect-free UiO-66 framework features relatively small cages, restricting the range of species that can be accommodated inside its porous structure or attached to the organic part of the framework *via* covalent or coordination bonds. The ordered removal of one cluster and twelve linkers leads to the formation of cages with a well-defined size of about 18 Å, approaching the mesoporous range, at the expense of the smaller pores having diameter of 7 Å and 9 Å. Besides increasing the gas storage capability, the presence of such big pores in UiO-66 offers several new opportunities for other applications that can involve larger species than small gaseous molecules, such as catalysis, drug delivery, sensing, photoactive materials. Focusing on catalysis, there are a number of potential advantages deriving from an ordered, missing-cluster defective framework. Diffusion limitations are likely to be reduced, granting guest species enough mobility to easily reach the active site, react and readily leave the reaction environment. The size range of the guest species themselves, either substrates or products, can be extended, allowing an increase in the complexity of the catalytic processes taking place inside the MOF. Similarly, the range of functional groups that can be attached to the linkers and accommodated inside the pores without obstructing them can be expanded. This has a tremendous importance for catalytic applications, where it can be of interest to graft onto the framework relatively bulky metal complexes that can act as single catalytic sites and mimic the behaviour of a homogeneous catalyst. By virtue of its stability, low cost, chemical versatility and large porosity, missing-cluster defective UiO-66 seems to have all the necessary features to be the ultimate MOF platform for catalysis.

PSM of defects has the potential to be a tremendously valuable addition to the toolbox of post-synthetic methods for functionalization of Zr-MOFs. Several approaches have been already investigated, producing strong proof of concepts and suggesting that defects can be a goldmine for modifying the physical-chemical properties of Zr-MOFs. The most straightforward way of taking advantage of defects is to perform SALI, i.e. exchange the species coordinated at defective sites with monocarboxylates bearing a functional group. The recent reports claiming that monocarboxylate-modulated UiO-66 might principally contain missing-cluster defects promote defective UiO-66 as an extremely intriguing and cost-effective matrix for SALI. As a matter of fact, it was recently shown that *L*-proline (*L*-pro, Chart 1) [59] and *L*-serine (*L*-ser, Chart 1) [126] can be efficiently introduced in defective UiO-66 employing facile post-synthetic routes. Similarly, oxalic acid was grafted to UiO-66, taking advantage of its smaller size if compared to H_2bdc, which prevented it from bridging two adjacent clusters, thus leaving a free -COOH group [180]. Interestingly, functional groups other than carboxylates were grafted to defective sites: in one case FA was substituted with sulphuric acid in MOF-808 [181], obtaining a super acidic material; in another example, phenylphosphonic acid was introduced in NU-1000, finding that the resulting material showed enhanced stability thanks to the

strong PO-Zr bonds [136]. Some pioneering articles were published on the post-synthetic metalation of defective sites on NU-1000 with Al and Zn [3], as well as V on defective UiO-66 [182], inspiring several other studies [19, 183-187] and further expanding the horizon of methods exploiting defects for the synthesis of functional Zr-MOFs. The observation that *L*-pro was incorporated at defective sites when it was used as a modulator [59] suggests that functionalization of defects could also be accomplished in a single-step manner, if functionalized monocarboxylic modulators were employed during the synthesis of the MOF. Particularly intriguing is the chemical diversity that can potentially be accessed by grafting functionalized monocarboxylates at defective sites, if compared with the limited range of functionalities that can be introduced in the framework as pendant groups of the linker.

The literature published so far probably just gives a hint of the vast landscape of chances for exploitation of defects in Zr-MOFs and it is easy to predict that a lot of work will be done in the near future to fully take advantage of the potential of defects for fine-tuning of the physical-chemical properties. Given the first ten years since the inception of Zr-MOFs chemistry have witnessed their impressive escalation to the Olympus of MOFs, the second decade might see their definitive establishment as the ultimate class of MOFs, combining high stability with large porosity and structural and chemical versatility, and manipulation of defects will arguably play a central role in this process.

ACKNOWLEDGEMENT

The author is supported by funding from the European Union's Horizon 2020 research and innovation programme under the Marie Skłodowska-Curie grant agreement No 663830. Prof. Andrew R. Barron, Dr. Enrico Andreoli, Dr. Russell J. Wakeham and Dr. Michael E. A. Warwick (ESRI) are gratefully acknowledged for proofreading the manuscript and helpful discussion.

REFERENCES

[1] J.H. Cavka, S. Jakobsen, U. Olsbye, N. Guillou, C. Lamberti, S. Bordiga, K.P. Lillerud, J. Am. Chem. Soc., 130 (2008) 13850-13851.
[2] Y. Bai, Y. Dou, L.H. Xie, W. Rutledge, J.R. Li, H.C. Zhou, Chem. Soc. Rev., 45 (2016) 2327-2367.
[3] J.E. Mondloch, W. Bury, D. Fairen-Jimenez, S. Kwon, E.J. DeMarco, M.H. Weston, A.A. Sarjeant, S.T. Nguyen, P.C. Stair, R.Q. Snurr, O.K. Farha, J.T. Hupp, J. Am. Chem. Soc., 135 (2013) 10294-10297.
[4] H. Furukawa, F. Gandara, Y.B. Zhang, J. Jiang, W.L. Queen, M.R. Hudson, O.M. Yaghi, J. Am. Chem. Soc., 136 (2014) 4369-4381.
[5] D. Feng, Z.Y. Gu, J.R. Li, H.L. Jiang, Z. Wei, H.C. Zhou, Angew. Chem. Int. Ed., 51 (2012) 10307-10310.
[6] V. Bon, V. Senkovskyy, I. Senkovska, S. Kaskel, Chem. Commun., 48 (2012) 8407-8409.
[7] F. Drache, V. Bon, I. Senkovska, J. Getzschmann, S. Kaskel, Philos. Trans. A Math. Phys. Eng. Sci., 375 (2017).
[8] J.B. DeCoste, G.W. Peterson, H. Jasuja, T.G. Glover, Y.-g. Huang, K.S. Walton, J. Mater. Chem. A, 1 (2013) 5642.
[9] N.C. Burtch, H. Jasuja, K.S. Walton, Chem. Rev., 114 (2014) 10575-10612.
[10] H. Wu, T. Yildirim, W. Zhou, J. Phys. Chem. Lett., 4 (2013) 925-930.
[11] C.L. Hobday, R.J. Marshall, C.F. Murphie, J. Sotelo, T. Richards, D.R. Allan, T. Duren, F.X. Coudert, R.S. Forgan, C.A. Morrison, S.A. Moggach, T.D. Bennett, Angew. Chem. Int. Ed., 55 (2016) 2401-2405.
[12] J. Ethiraj, E. Albanese, B. Civalleri, J.G. Vitillo, F. Bonino, S. Chavan, G.C. Shearer, K.P. Lillerud, S. Bordiga, ChemSusChem, 7 (2014) 3382-3388.
[13] M. Ganesh, P. Hemalatha, M.M. Peng, W.S. Cha, H.T. Jang, Aerosol Air. Qual. Res., 14 (2014) 1605-1612.
[14] H. Huang, W. Zhang, F. Yang, B. Wang, Q. Yang, Y. Xie, C. Zhong, J.-R. Li, Chem. Eng. J., 289 (2016) 247-253.
[15] H.R. Abid, J. Shang, H.-M. Ang, S. Wang, Int. J. Smart Nano Mater., 4 (2013) 72-82.
[16] B. Wang, H. Huang, X.-L. Lv, Y. Xie, M. Li, J.-R. Li, Inorg. Chem., 53 (2014) 9254-9259.
[17] M. Rimoldi, A.J. Howarth, M.R. DeStefano, L. Lin, S. Goswami, P. Li, J.T. Hupp, O.K. Farha, ACS Catal., 7 (2016) 997-1014.
[18] H. Fei, S.M. Cohen, Chem. Commun., 50 (2014) 4810-4812.
[19] R.C. Klet, S. Tussupbayev, J. Borycz, J.R. Gallagher, M.M. Stalzer, J.T. Miller, L. Gagliardi, J.T. Hupp, T.J. Marks, C.J. Cramer, M. Delferro, O.K. Farha, J. Am. Chem. Soc., 137 (2015) 15680-15683.
[20] S. Pullen, H. Fei, A. Orthaber, S.M. Cohen, S. Ott, J. Am. Chem. Soc., 135 (2013) 16997-17003.
[21] F. Vermoortele, R. Ameloot, A. Vimont, C. Serre, D. De Vos, Chem. Commun., 47 (2011) 1521-1523.
[22] M. Filippousi, S. Turner, K. Leus, P.I. Siafaka, E.D. Tseligka, M. Vandichel, S.G. Nanaki, I.S. Vizirianakis, D.N. Bikiaris, P. Van Der Voort, G. Van Tendeloo, Int. J. Pharm., 509 (2016) 208-218.
[23] C. Orellana-Tavra, E.F. Baxter, T. Tian, T.D. Bennett, N.K. Slater, A.K. Cheetham, D. Fairen-Jimenez, Chem. Commun., 51 (2015) 13878-13881.
[24] D. Cunha, M. Ben Yahia, S. Hall, S.R. Miller, H. Chevreau, E. Elkaïm, G. Maurin, P. Horcajada, C. Serre, Chem. Mater., 25 (2013) 2767-2776.
[25] C. Orellana-Tavra, S.A. Mercado, D. Fairen-Jimenez, Adv. Healthc. Mater., 5 (2016) 2261-2270.
[26] K.A. Mocniak, I. Kubajewska, D.E.M. Spillane, G.R. Williams, R.E. Morris, RSC Adv., 5 (2015) 83648-83656.
[27] Z. Hu, X. Jiang, F. Xu, J. Jia, Z. Long, X. Hou, Talanta, 158 (2016) 276-282.
[28] B. Wang, X.-L. Lv, D. Feng, L.-H. Xie, J. Zhang, M. Li, Y. Xie, J.-R. Li, H.-C. Zhou, J. Am. Chem. Soc., 138 (2016) 6204-6216.
[29] G. Nickerl, I. Senkovska, S. Kaskel, Chem. Commun., 51 (2015) 2280-2282.
[30] H.-T. Zhang, J.-W. Zhang, G. Huang, Z.-Y. Du, H.-L. Jiang, Chem. Commun., 50 (2014) 12069-12072.

[31] Z. Xu, L. Yang, C. Xu, Anal. Chem., 87 (2015) 3438-3444.
[32] B. Wang, Q. Yang, C. Guo, Y. Sun, L.-H. Xie, J.-R. Li, ACS Applied Materials & Interfaces, 9 (2017) 10286-10295.
[33] I. Hod, P. Deria, W. Bury, J.E. Mondloch, C.W. Kung, M. So, M.D. Sampson, A.W. Peters, C.P. Kubiak, O.K. Farha, J.T. Hupp, Nat. Comm., 6 (2015) 8304.
[34] I. Stassen, M. Styles, T. Van Assche, N. Campagnol, J. Fransaer, J. Denayer, J.-C. Tan, P. Falcaro, D. De Vos, R. Ameloot, Chem. Mater., 27 (2015) 1801-1807.
[35] Y. Tan, W. Zhang, Y. Gao, J. Wu, B. Tang, RSC Adv., 5 (2015) 17601-17605.
[36] W. Zhang, J. Chen, Y. Li, W. Yang, Y. Zhang, Y. Zhang, RSC Adv., 7 (2017) 5628-5635.
[37] Z. Hu, D. Zhao, Dalton Trans., 44 (2015) 19018-19040.
[38] H. Reinsch, S. Waitschat, S.M. Chavan, K.P. Lillerud, N. Stock, Eur. J. Inorg. Chem., 2016 (2016) 4490-4498.
[39] Z. Hu, I. Castano, S. Wang, Y. Wang, Y. Peng, Y. Qian, C. Chi, X. Wang, D. Zhao, Cryst. Growth Des., 16 (2016) 2295-2301.
[40] Z. Hu, Y. Peng, Z. Kang, Y. Qian, D. Zhao, Inorg. Chem., 54 (2015) 4862-4868.
[41] H. Reinsch, Eur. J. Inorg. Chem., 2016 (2016) 4290-4299.
[42] A.M. Ploskonka, S.E. Marzen, J.B. DeCoste, Ind. Eng. Chem. Res., 56 (2017) 1478-1484.
[43] J. Zhang, G.B. White, M.D. Ryan, A.J. Hunt, M.J. Katz, ACS Sust. Chem. Eng., 4 (2016) 7186-7192.
[44] M. Taddei, P.V. Dau, S.M. Cohen, M. Ranocchiari, J.A. van Bokhoven, F. Costantino, S. Sabatini, R. Vivani, Dalton Trans., 44 (2015) 14019-14026.
[45] Y. Li, Y. Liu, W. Gao, L. Zhang, W. Liu, J. Lu, Z. Wang, Y.-J. Deng, CrystEngComm, 16 (2014) 7037.
[46] W. Liang, C.J. Coghlan, F. Ragon, M. Rubio-Martinez, D.M. D'Alessandro, R. Babarao, Dalton Trans., 45 (2016) 4496-4500.
[47] J. Ren, T. Segakweng, H. Langmi, N. Musyoka, B. North, M. Mathe, D. Bessarabov, Int. J. Mater. Res., 105 (2014) 516-519.
[48] K. Uzarevic, T.C. Wang, S.Y. Moon, A.M. Fidelli, J.T. Hupp, O.K. Farha, T. Friscic, Chem. Commun., 52 (2016) 2133-2136.
[49] C. Zou, S. Vagin, A. Kronast, B. Rieger, RSC Adv., 6 (2016) 102968-102971.
[50] K.B. Lausund, O. Nilsen, Nat. Comm., 7 (2016) 13578.
[51] A. Carne-Sanchez, I. Imaz, M. Cano-Sarabia, D. Maspoch, Nat. Chem., 5 (2013) 203-211.
[52] M. Rubio-Martinez, M.P. Batten, A. Polyzos, K.C. Carey, J.I. Mardel, K.S. Lim, M.R. Hill, Sci. Rep., 4 (2014) 5443.
[53] M. Taddei, D.A. Steitz, J.A. van Bokhoven, M. Ranocchiari, Chem. Eur. J., 22 (2016) 3245-3249.
[54] S. Waitschat, M.T. Wharmby, N. Stock, Dalton Trans., 44 (2015) 11235-11240.
[55] S. Tai, W. Zhang, J. Zhang, G. Luo, Y. Jia, M. Deng, Y. Ling, Microporous Mesoporous Mater., 220 (2016) 148-154.
[56] A. Polyzoidis, M. Schwarzer, S. Loebbecke, C.G. Piscopo, Mater. Lett., (2017).
[57] A. Schaate, P. Roy, A. Godt, J. Lippke, F. Waltz, M. Wiebcke, P. Behrens, Chem. Eur. J., 17 (2011) 6643-6651.
[58] R.J. Marshall, C.L. Hobday, C.F. Murphie, S.L. Griffin, C.A. Morrison, S.A. Moggach, R.S. Forgan, J. Mater. Chem. A, 4 (2016) 6955-6963.
[59] O.V. Gutov, S. Molina, E.C. Escudero-Adan, A. Shafir, Chem. Eur. J., 22 (2016) 13582-13587.
[60] M. Taddei, K.C. Dumbgen, J.A. van Bokhoven, M. Ranocchiari, Chem. Commun., 52 (2016) 6411-6414.
[61] S. Øien, D. Wragg, H. Reinsch, S. Svelle, S. Bordiga, C. Lamberti, K.P. Lillerud, Cryst. Growth Des., 14 (2014) 5370-5372.
[62] M.J. Katz, Z.J. Brown, Y.J. Colon, P.W. Siu, K.A. Scheidt, R.Q. Snurr, J.T. Hupp, O.K. Farha, Chem. Commun., 49 (2013) 9449-9451.
[63] Y. Han, M. Liu, K. Li, Y. Zuo, Y. Wei, S. Xu, G. Zhang, C. Song, Z. Zhang, X. Guo, CrystEngComm, 17 (2015) 6434-6440.
[64] V. Bon, I. Senkovska, M.S. Weiss, S. Kaskel, CrystEngComm, 15 (2013) 9572.

[65] M. Kandiah, M.H. Nilsen, S. Usseglio, S. Jakobsen, U. Olsbye, M. Tilset, C. Larabi, E.A. Quadrelli, F. Bonino, K.P. Lillerud, Chem. Mater., 22 (2010) 6632-6640.
[66] S. Biswas, J. Zhang, Z. Li, Y.Y. Liu, M. Grzywa, L. Sun, D. Volkmer, P. Van Der Voort, Dalton Trans., 42 (2013) 4730-4737.
[67] S. Biswas, P. Van Der Voort, Eur. J. Inorg. Chem., 2013 (2013) 2154-2160.
[68] F. Ragon, B. Campo, Q. Yang, C. Martineau, A.D. Wiersum, A. Lago, V. Guillerm, C. Hemsley, J.F. Eubank, M. Vishnuvarthan, F. Taulelle, P. Horcajada, A. Vimont, P.L. Llewellyn, M. Daturi, S. Devautour-Vinot, G. Maurin, C. Serre, T. Devic, G. Clet, J. Mater. Chem. A, 3 (2015) 3294-3309.
[69] S.M. Chavan, G.C. Shearer, S. Svelle, U. Olsbye, F. Bonino, J. Ethiraj, K.P. Lillerud, S. Bordiga, Inorg. Chem., 53 (2014) 9509-9515.
[70] Y. Sun, L. Sun, D. Feng, H.C. Zhou, Angew. Chem. Int. Ed., 55 (2016) 6471-6475.
[71] C.H. Hendon, J. Bonnefoy, E.A. Quadrelli, J. Canivet, M.B. Chambers, G. Rousse, A. Walsh, M. Fontecave, C. Mellot-Draznieks, Chem. Eur. J., 22 (2016) 3713-3718.
[72] M. Taddei, D. Tiana, N. Casati, J.A. van Bokhoven, B. Smit, M. Ranocchiari, Phys. Chem. Chem. Phys., 19 (2017) 1551-1559.
[73] S. Yuan, J.S. Qin, L. Zou, Y.P. Chen, X. Wang, Q. Zhang, H.C. Zhou, J. Am. Chem. Soc., 138 (2016) 6636-6642.
[74] M. Lin Foo, S. Horike, T. Fukushima, Y. Hijikata, Y. Kubota, M. Takata, S. Kitagawa, Dalton Trans., 41 (2012) 13791-13794.
[75] T.L. Doan, T.Q. Dao, H.N. Tran, P.H. Tran, T.N. Le, Dalton Trans., 45 (2016) 7875-7880.
[76] R.J. Marshall, R.S. Forgan, Eur. J. Inorg. Chem., 2016 (2016) 4310-4331.
[77] M. Kim, S.J. Garibay, S.M. Cohen, Inorg. Chem., 50 (2011) 729-731.
[78] M. Kandiah, S. Usseglio, S. Svelle, U. Olsbye, K.P. Lillerud, M. Tilset, J. Mater. Chem., 20 (2010) 9848.
[79] F.G. Xi, H. Liu, N.N. Yang, E.Q. Gao, Inorg. Chem., 55 (2016) 4701-4703.
[80] M. Kim, J.F. Cahill, Y. Su, K.A. Prather, S.M. Cohen, Chem. Sci., 3 (2012) 126-130.
[81] H. Fei, S.M. Cohen, J. Am. Chem. Soc., 137 (2015) 2191-2194.
[82] H. Fei, J. Shin, Y.S. Meng, M. Adelhardt, J. Sutter, K. Meyer, S.M. Cohen, J. Am. Chem. Soc., 136 (2014) 4965-4973.
[83] M. Kim, J.F. Cahill, H. Fei, K.A. Prather, S.M. Cohen, J. Am. Chem. Soc., 134 (2012) 18082-18088.
[84] C.H. Lau, R. Babarao, M.R. Hill, Chem. Commun., 49 (2013) 3634-3636.
[85] A.M. Rasero-Almansa, M. Iglesias, F. Sánchez, RSC Adv., 6 (2016) 106790-106797.
[86] Z. Fang, B. Bueken, D.E. De Vos, R.A. Fischer, Angew. Chem. Int. Ed., 54 (2015) 7234-7254.
[87] A.K. Cheetham, T.D. Bennett, F.X. Coudert, A.L. Goodwin, Dalton Trans., 45 (2016) 4113-4126.
[88] A.B. Cairns, A.L. Goodwin, Chem. Soc. Rev., 42 (2013) 4881-4893.
[89] T.D. Bennett, A.K. Cheetham, A.H. Fuchs, F.-X. Coudert, Nat. Chem., 9 (2017) 11-16.
[90] L. Valenzano, B. Civalleri, S. Chavan, S. Bordiga, M.H. Nilsen, S. Jakobsen, K.P. Lillerud, C. Lamberti, Chem. Mater., 23 (2011) 1700-1718.
[91] H. Wu, Y.S. Chua, V. Krungleviciute, M. Tyagi, P. Chen, T. Yildirim, W. Zhou, J. Am. Chem. Soc., 135 (2013) 10525-10532.
[92] M.J. Cliffe, W. Wan, X. Zou, P.A. Chater, A.K. Kleppe, M.G. Tucker, H. Wilhelm, N.P. Funnell, F.X. Coudert, A.L. Goodwin, Nat. Comm., 5 (2014) 4176.
[93] G.C. Shearer, S. Chavan, S. Bordiga, S. Svelle, U. Olsbye, K.P. Lillerud, Chem. Mater., 28 (2016) 3749-3761.
[94] C.A. Trickett, K.J. Gagnon, S. Lee, F. Gandara, H.B. Burgi, O.M. Yaghi, Angew. Chem. Int. Ed., 54 (2015) 11162-11167.
[95] G.C. Shearer, S. Chavan, J. Ethiraj, J.G. Vitillo, S. Svelle, U. Olsbye, C. Lamberti, S. Bordiga, K.P. Lillerud, Chem. Mater., 26 (2014) 4068-4071.
[96] W. Liang, H. Chevreau, F. Ragon, P.D. Southon, V.K. Peterson, D.M. D'Alessandro, CrystEngComm, 16 (2014) 6530.
[97] P. Ghosh, Y.J. Colon, R.Q. Snurr, Chem. Commun., 50 (2014) 11329-11331.

[98] A.J. Howarth, Y. Liu, P. Li, Z. Li, T.C. Wang, J.T. Hupp, O.K. Farha, Nat. Rev. Mater., 1 (2016) 15018.
[99] M.J. Cliffe, J.A. Hill, C.A. Murray, F.X. Coudert, A.L. Goodwin, Phys. Chem. Chem. Phys., 17 (2015) 11586-11592.
[100] J.C. Tan, A.K. Cheetham, Chem. Soc. Rev., 40 (2011) 1059-1080.
[101] P.G. Yot, K. Yang, F. Ragon, V. Dmitriev, T. Devic, P. Horcajada, C. Serre, G. Maurin, Dalton Trans., 45 (2016) 4283-4288.
[102] T.D. Bennett, T.K. Todorova, E.F. Baxter, D.G. Reid, C. Gervais, B. Bueken, B. Van de Voorde, D. De Vos, D.A. Keen, C. Mellot-Draznieks, Phys. Chem. Chem. Phys., 18 (2016) 2192-2201.
[103] A.W. Thornton, R. Babarao, A. Jain, F. Trousselet, F.X. Coudert, Dalton Trans., 45 (2016) 4352-4359.
[104] B. Van de Voorde, I. Stassen, B. Bueken, F. Vermoortele, D. De Vos, R. Ameloot, J.-C. Tan, T.D. Bennett, J. Mater. Chem. A, 3 (2015) 1737-1742.
[105] S.M. Rogge, J. Wieme, L. Vanduyfhuys, S. Vandenbrande, G. Maurin, T. Verstraelen, M. Waroquier, V. Van Speybroeck, Chem. Mater., 28 (2016) 5721-5732.
[106] P.L. Llewellyn, S. Bourrelly, C. Serre, A. Vimont, M. Daturi, L. Hamon, G. De Weireld, J.S. Chang, D.Y. Hong, Y. Kyu Hwang, S. Hwa Jhung, G. Ferey, Langmuir, 24 (2008) 7245-7250.
[107] P.D.C. Dietzel, V. Besikiotis, R. Blom, J. Mater. Chem., 19 (2009) 7362.
[108] Z. Hu, D. Zhao, CrystEngComm, (2017).
[109] S. Horike, M. Dinca, K. Tamaki, J.R. Long, J. Am. Chem. Soc., 130 (2008) 5854-5855.
[110] G.C. Shearer, S. Forselv, S. Chavan, S. Bordiga, K. Mathisen, M. Bjørgen, S. Svelle, K.P. Lillerud, Top. Catal., 56 (2013) 770-782.
[111] F. Vermoortele, M. Vandichel, B. Van de Voorde, R. Ameloot, M. Waroquier, V. Van Speybroeck, D.E. De Vos, Angew. Chem. Int. Ed., 51 (2012) 4887-4890.
[112] F. Vermoortele, B. Bueken, G. Le Bars, B. Van de Voorde, M. Vandichel, K. Houthoofd, A. Vimont, M. Daturi, M. Waroquier, V. Van Speybroeck, C. Kirschhock, D.E. De Vos, J. Am. Chem. Soc., 135 (2013) 11465-11468.
[113] M. Vandichel, J. Hajek, F. Vermoortele, M. Waroquier, D.E. De Vos, V. Van Speybroeck, CrystEngComm, 17 (2015) 395-406.
[114] J.E. Mondloch, M.J. Katz, W.C. Isley, 3rd, P. Ghosh, P. Liao, W. Bury, G.W. Wagner, M.G. Hall, J.B. DeCoste, G.W. Peterson, R.Q. Snurr, C.J. Cramer, J.T. Hupp, O.K. Farha, Nat. Mater., 14 (2015) 512-516.
[115] M.J. Katz, R.C. Klet, S.-Y. Moon, J.E. Mondloch, J.T. Hupp, O.K. Farha, ACS Catal., 5 (2015) 4637-4642.
[116] Y. Zang, J. Shi, F. Zhang, Y. Zhong, W. Zhu, Catal. Sci. Technol., 3 (2013) 2044-2049.
[117] C. Lieder, S. Opelt, M. Dyballa, H. Henning, E. Klemm, M. Hunger, J. Phys. Chem. C, 114 (2010) 16596-16602.
[118] G.K.H. Shimizu, J.M. Taylor, S. Kim, Science, 341 (2013) 354.
[119] J. Jiang, O.M. Yaghi, Chem. Rev., 115 (2015) 6966-6997.
[120] R.C. Klet, Y. Liu, T.C. Wang, J.T. Hupp, O.K. Farha, J. Mater. Chem. A, 4 (2016) 1479-1485.
[121] Y. Liu, R.C. Klet, J.T. Hupp, O. Farha, Chem. Commun., 52 (2016) 7806-7809.
[122] J.M. Taylor, S. Dekura, R. Ikeda, H. Kitagawa, Chem. Mater., 27 (2015) 2286-2289.
[123] J.K. Bristow, K.L. Svane, D. Tiana, J.M. Skelton, J.D. Gale, A. Walsh, J. Phys. Chem. C, 120 (2016) 9276-9281.
[124] A. Paul, D. Connolly, M. Schulz, M.T. Pryce, J.G. Vos, Inorg. Chem., 51 (2012) 1977-1979.
[125] T. Cottineau, M. Richard-Plouet, J.-Y. Mevellec, L. Brohan, J. Phys. Chem. C, 115 (2011) 12269-12274.
[126] G.C. Shearer, J.G. Vitillo, S. Bordiga, S. Svelle, U. Olsbye, K.P. Lillerud, Chem. Mater., 28 (2016) 7190-7193.
[127] K. Wang, C. Li, Y. Liang, T. Han, H. Huang, Q. Yang, D. Liu, C. Zhong, Chem. Eng. J., 289 (2016) 486-493.

[128] O.V. Gutov, M. Gonzalez Hevia, E.C. Escudero-Adan, A. Shafir, Inorg. Chem., 54 (2015) 8396-8400.
[129] S. Ling, B. Slater, Chem. Sci., 7 (2016) 4706-4712.
[130] M. Vandichel, J. Hajek, A. Ghysels, A. De Vos, M. Waroquier, V. Van Speybroeck, CrystEngComm, 18 (2016) 7056-7069.
[131] M. Taddei, P. Sassi, F. Costantino, R. Vivani, Inorg. Chem., 55 (2016) 6278-6285.
[132] M. Taddei, R. Vivani, F. Costantino, Dalton Trans., 42 (2013) 9671-9678.
[133] F. Costantino, P. Sassi, M. Geppi, M. Taddei, Cryst. Growth Des., 12 (2012) 5462-5470.
[134] M. Taddei, F. Costantino, V. Manuali, R. Vivani, Inorg. Chem., 50 (2011) 10835-10843.
[135] P. Deria, W. Bury, J.T. Hupp, O.K. Farha, Chem. Commun., 50 (2014) 1965-1968.
[136] P. Deria, W. Bury, I. Hod, C.-W. Kung, O. Karagiaridi, J.T. Hupp, O.K. Farha, Inorg. Chem., 54 (2015) 2185-2192.
[137] S. Yuan, W. Lu, Y.P. Chen, Q. Zhang, T.F. Liu, D. Feng, X. Wang, J. Qin, H.C. Zhou, J. Am. Chem. Soc., 137 (2015) 3177-3180.
[138] S. Yuan, Y.P. Chen, J.S. Qin, W. Lu, L. Zou, Q. Zhang, X. Wang, X. Sun, H.C. Zhou, J. Am. Chem. Soc., 138 (2016) 8912-8919.
[139] C.X. Chen, Z. Wei, J.J. Jiang, Y.Z. Fan, S.P. Zheng, C.C. Cao, Y.H. Li, D. Fenske, C.Y. Su, Angew. Chem. Int. Ed., 55 (2016) 9932-9936.
[140] F.R. Kogler, M. Jupa, M. Puchberger, U. Schubert, J. Mater. Chem., 14 (2004) 3133-3138.
[141] M. Puchberger, F.R. Kogler, M. Jupa, S. Gross, H. Fric, G. Kickelbick, U. Schubert, Eur. J. Inorg. Chem., 2006 (2006) 3283-3293.
[142] P. Walther, M. Puchberger, F.R. Kogler, K. Schwarz, U. Schubert, Phys. Chem. Chem. Phys., 11 (2009) 3640-3647.
[143] J. Juan-Alcañiz, R. Gielisse, A.B. Lago, E.V. Ramos-Fernandez, P. Serra-Crespo, T. Devic, N. Guillou, C. Serre, F. Kapteijn, J. Gascon, Catal. Sci. Technol., 3 (2013) 2311.
[144] J.M. Taylor, T. Komatsu, S. Dekura, K. Otsubo, M. Takata, H. Kitagawa, J. Am. Chem. Soc., 137 (2015) 11498-11506.
[145] X. Yang, A.E. Clark, Inorg. Chem., 53 (2014) 8930-8940.
[146] M.G. Goesten, P.C.M.M. Magusin, E.A. Pidko, B. Mezari, E.J.M. Hensen, F. Kapteijn, J. Gascon, Inorg. Chem., 53 (2014) 882-887.
[147] E. Stavitski, M. Goesten, J. Juan-Alcañiz, A. Martinez-Joaristi, P. Serra-Crespo, A.V. Petukhov, J. Gascon, F. Kapteijn, Angew. Chem. Int. Ed., 50 (2011) 9624-9628.
[148] D.C. Cantu, B.P. McGrail, V.-A. Glezakou, Chem. Mater., 26 (2014) 6401-6409.
[149] M. Haouas, C. Volkringer, T. Loiseau, G. Férey, F. Taulelle, Chem. Mater., 24 (2012) 2462-2471.
[150] G. Férey, M. Haouas, T. Loiseau, F. Taulelle, Chem. Mater., 26 (2014) 299-309.
[151] F. Millange, M.I. Medina, N. Guillou, G. Férey, K.M. Golden, R.I. Walton, Angew. Chem. Int. Ed., 49 (2010) 763-766.
[152] J. Cravillon, C.A. Schröder, H. Bux, A. Rothkirch, J. Caro, M. Wiebcke, CrystEngComm, 14 (2012) 492-498.
[153] P.Y. Moh, M. Brenda, M.W. Anderson, M.P. Attfield, CrystEngComm, 15 (2013) 9672-9678.
[154] J. Cravillon, C.A. Schröder, R. Nayuk, J. Gummel, K. Huber, M. Wiebcke, Angew. Chem. Int. Ed., 123 (2011) 8217-8221.
[155] P.Y. Moh, P. Cubillas, M.W. Anderson, M.P. Attfield, J. Am. Chem. Soc., 133 (2011) 13304-13307.
[156] M. Shoaee, M.W. Anderson, M.P. Attfield, Angew. Chem. Int. Ed., 120 (2008) 8653-8656.
[157] M. Shoaee, J.R. Agger, M.W. Anderson, M.P. Attfield, CrystEngComm, 10 (2008) 646-648.
[158] N.S. John, C. Scherb, M. Shoaee, M.W. Anderson, M.P. Attfield, T. Bein, Chem. Commun., (2009) 6294-6296.
[159] D. Zacher, R. Nayuk, R. Schweins, R.A. Fischer, K. Huber, Cryst. Growth Des., 14 (2014) 4859-4863.

[160] S. Hermes, T. Witte, T. Hikov, D. Zacher, S. Bahnmüller, G. Langstein, K. Huber, R.A. Fischer, J. Am. Chem. Soc., 129 (2007) 5324-5325.
[161] J. Kim, M.R. Dolgos, B.J. Lear, Cryst. Growth Des., 15 (2015) 4781-4786.
[162] P. Cubillas, K. Etherington, M.W. Anderson, M.P. Attfield, CrystEngComm, 16 (2014) 9834-9841.
[163] P. Cubillas, M.W. Anderson, M.P. Attfield, Chem. Eur. J., 18 (2012) 15406-15415.
[164] D. Biswal, P.G. Kusalik, ACS nano, 11 (2017) 258-268.
[165] R.I. Walton, F. Millange, In Situ Studies of the Crystallization of Metal–Organic Frameworks, in: S. Kaskel (Ed.) The Chemistry of Metal–Organic Frameworks: Synthesis, Characterization, and Applications, Wiley-VCH Verlag GmbH & Co. KGaA, Weinheim, 2016, pp. 729-764.
[166] F. Ragon, P. Horcajada, H. Chevreau, Y.K. Hwang, U.H. Lee, S.R. Miller, T. Devic, J.S. Chang, C. Serre, Inorg. Chem., 53 (2014) 2491-2500.
[167] G. Zahn, P. Zerner, J. Lippke, F.L. Kempf, S. Lilienthal, C.A. Schröder, A.M. Schneider, P. Behrens, CrystEngComm, 16 (2014) 9198-9207.
[168] M.G. Goesten, M.F. de Lange, A.I. Olivos-Suarez, A.V. Bavykina, P. Serra-Crespo, C. Krywka, F.M. Bickelhaupt, F. Kapteijn, J. Gascon, Nat. Comm., 7 (2016) 11832.
[169] D.J. Tranchemontagne, J.L. Mendoza-Cortes, M. O'Keeffe, O.M. Yaghi, Chem. Soc. Rev., 38 (2009) 1257-1283.
[170] M. Eddaoudi, D.B. Moler, H. Li, B. Chen, T.M. Reineke, M. O'Keeffe, O.M. Yaghi, Acc. Chem. Res., 34 (2001) 319-330.
[171] C.K. Brozek, V.K. Michaelis, T.-C. Ong, L. Bellarosa, N. López, R.G. Griffin, M. Dincă, ACS Cent. Sci., 1 (2015) 252-260.
[172] Z. Akimbekov, D. Wu, C.K. Brozek, M. Dinca, A. Navrotsky, Phys. Chem. Chem. Phys., 18 (2016) 1158-1162.
[173] Y.Y. Kharitonov, M.M. Bekhit, S.F. Belevskij, Koordinats. Khim., 6 (1980) 1548-1559.
[174] S.I. Troyanov, G.N. Mazo, B.V. Merinov, B.A. Maksimov, Kristallografiya, 34 (1989) 235-237.
[175] W. Errington, M.A. Ismail, Acta Crystallogr. Sect. C-Cryst. Struct. Commun., 50 (1994) 1540-1541.
[176] S.L. Benjamin, W. Levason, D. Pugh, G. Reid, W. Zhang, Dalton Trans., 41 (2012) 12548-12557.
[177] G. Kickelbick, M.P. Feth, H. Bertagnolli, M. Puchberger, D. Holzinger, S. Gross, J. Chem. Soc. Dalton Trans., (2002) 3892-3898.
[178] G. Kickelbick, P. Wiede, U. Schubert, Inorg. Chim. Acta, 284 (1999) 1-7.
[179] M.R. DeStefano, T. Islamoglu, S.J. Garibay, J.T. Hupp, O.K. Farha, Chem. Mater., 29 (2017) 1357-1361.
[180] J.B. DeCoste, T.J. Demasky, M.J. Katz, O.K. Farha, J.T. Hupp, New J. Chem., 39 (2015) 2396-2399.
[181] J. Jiang, F. Gandara, Y.B. Zhang, K. Na, O.M. Yaghi, W.G. Klemperer, J. Am. Chem. Soc., 136 (2014) 12844-12847.
[182] H.G.T. Nguyen, N.M. Schweitzer, C.-Y. Chang, T.L. Drake, M.C. So, P.C. Stair, O.K. Farha, J.T. Hupp, S.T. Nguyen, ACS Catal., 4 (2014) 2496-2500.
[183] S. Yuan, Y.P. Chen, J. Qin, W. Lu, X. Wang, Q. Zhang, M. Bosch, T.F. Liu, X. Lian, H.C. Zhou, Angew. Chem. Int. Ed., 54 (2015) 14696-14700.
[184] T.-F. Liu, N.A. Vermeulen, A.J. Howarth, P. Li, A.A. Sarjeant, J.T. Hupp, O.K. Farha, Eur. J. Inorg. Chem., 2016 (2016) 4349-4352.
[185] Z. Li, A.W. Peters, V. Bernales, M.A. Ortuno, N.M. Schweitzer, M.R. DeStefano, L.C. Gallington, A.E. Platero-Prats, K.W. Chapman, C.J. Cramer, L. Gagliardi, J.T. Hupp, O.K. Farha, ACS Cent. Sci., 3 (2017) 31-38.
[186] H. Noh, Y. Cui, A.W. Peters, D.R. Pahls, M.A. Ortuno, N.A. Vermeulen, C.J. Cramer, L. Gagliardi, J.T. Hupp, O.K. Farha, J. Am. Chem. Soc., 138 (2016) 14720-14726.
[187] A.W. Peters, Z. Li, O.K. Farha, J.T. Hupp, ACS nano, 9 (2015) 8484-8490.

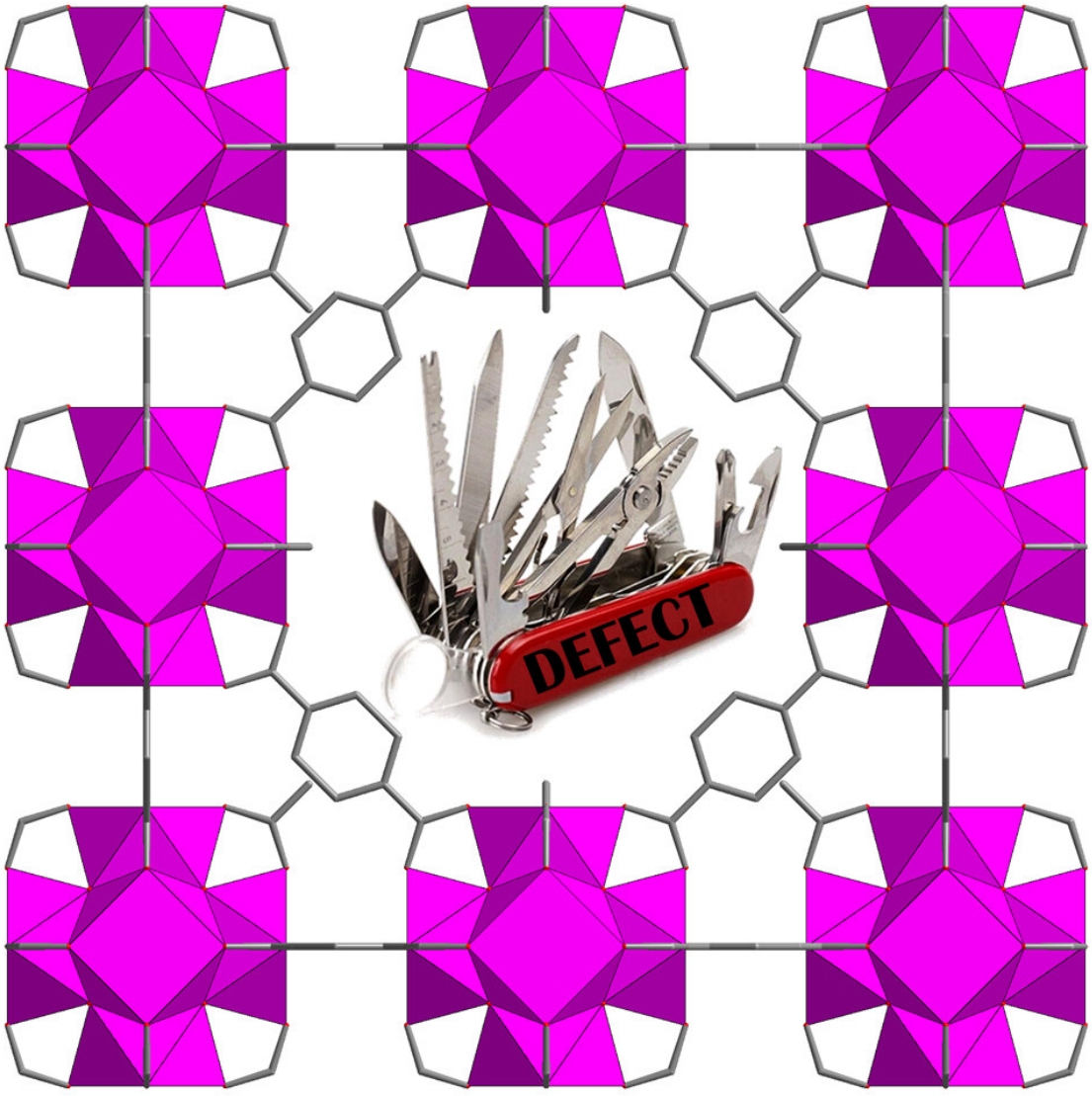

Graphical abstract

HIGHLIGHTS

- Zr-MOFs can contain many defects without suffering from loss of stability
- Defects significantly influence the physical-chemical properties of Zr-MOFs
- Gaps exist in the understanding of fundamental aspects of defects in Zr-MOFs
- Defects offer new opportunities for functionalization of Zr-MOFs